The Syp1/FCHo2 protein induces septin filament bundling through its intrinsically disordered domain

Sandy Ibanes, Fatima El Alaoui, Josephine Lai Kee Him, Chantal Cazevieille,
François Hoh, Sébastien Lyonnais, Patrick Bron, Luca Cipelletti, Laura Picas,
Simonetta Piatti

The Syp1/FCHo2 protein induces septin filament bundling through its intrinsically disordered domain

Graphical abstract
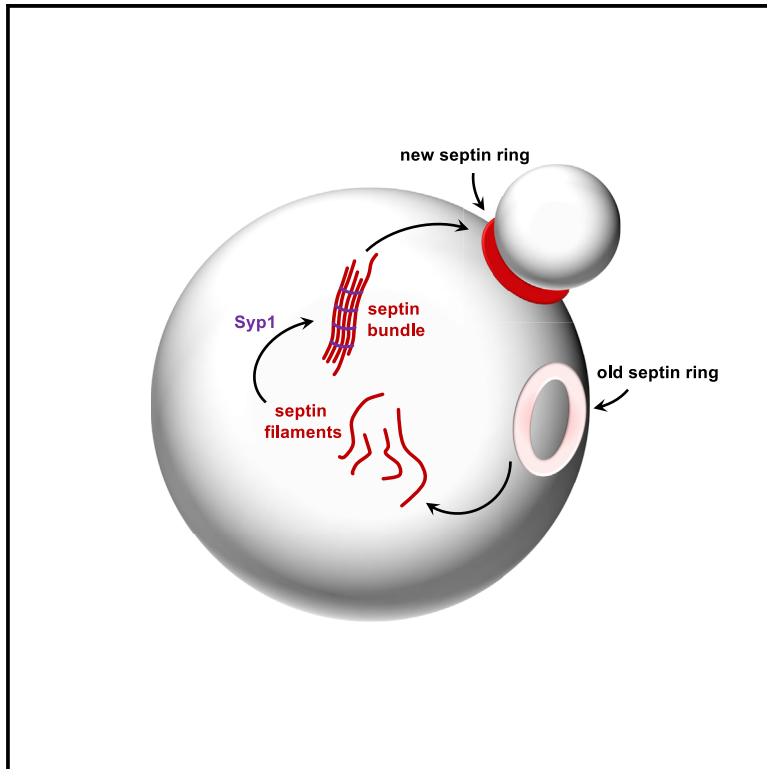
Authors

Sandy Ibanes, Fatima El-Alaoui,
Joséphine Lai-Kee-Him, ...,
Luca Cipelletti, Laura Picas,
Simonetta Piatti

Correspondence

simonetta.piatti@crbm.cnrs.fr

In brief

A septin collar at the division site is essential for budding yeast cytokinesis. Yet, how it gets organized is not understood. Using *in vitro* reconstitution assays, Ibanes et al. show that the F-BAR protein Syp1 aligns and bundles septin filaments into ordered arrays, thereby contributing to septin collar assembly.

Highlights

- The budding yeast F-BAR protein Syp1 promotes septin recycling

- Syp1 induces septin filament bundling *in vitro*

- The septin-bundling activity of Syp1 is shared by its mammalian counterpart FCHo2

- Septin bundling relies mainly on the intrinsically disordered domain of Syp1

Article

The Syp1/FCHo2 protein induces septin filament bundling through its intrinsically disordered domain

Sandy Ibanes,[1] Fatima El-Alaoui,[2] Joséphine Lai-Kee-Him,[3] Chantal Cazevieille,[4] François Hoh,[3] Sébastien Lyonnais,[5] Patrick Bron,[3] Luca Cipelletti,[6,7] Laura Picas,[2] and Simonetta Piatti[1,8,*]

[1]CRBM (Centre de Recherche en Biologie cellulaire de Montpellier), University of Montpellier, CNRS UMR 5237, 1919 Route de Mende, 34293 Montpellier, France
[2]IRIM (Institut de Recherche en Infectiologie de Montpellier), University of Montpellier, CNRS UMR 9004, 1919 Route de Mende, 34293 Montpellier, France
[3]CBS (Centre de Biologie Structurale), University of Montpellier, CNRS UMR 5048, INSERM U 1054, 29 Rue de Navacelles, 34090 Montpellier, France
[4]COMET Electron Microscopy Platform, INM (Institute for Neurosciences of Montpellier), University of Montpellier, INSERM U 1298, 80 Rue Augustin Fliche, 34091 Montpellier, France
[5]CEMIPAI (Centre d'Etudes des Maladies Infectieuses et Pharmacologie Anti-Infectieuse), University of Montpellier, UAR 3725 CNRS, Montpellier, France
[6]L2C (Laboratoire Charles Coulomb), University of Montpellier, CNRS, Place E. Bataillon, 34095 Montpellier, France
[7]IUF (Institut Universitaire de France), Paris, France
[8]Lead contact
*Correspondence: simonetta.piatti@crbm.cnrs.fr
https://doi.org/10.1016/j.celrep.2022.111765

SUMMARY

The septin collar of budding yeast is an ordered array of septin filaments that serves a scaffolding function for the cytokinetic machinery at the bud neck and compartmentalizes the membrane between mother and daughter cell. How septin architecture is aided by septin-binding proteins is largely unknown. Syp1 is an endocytic protein that was implicated in the timely recruitment of septins to the newly forming collar through an unknown mechanism. Using advanced microscopy and *in vitro* reconstitution assays, we show that Syp1 is able to align laterally and tightly pack septin filaments, thereby forming flat bundles or sheets. This property is shared by the Syp1 mammalian counterpart FCHo2, thus emphasizing conserved protein functions. Interestingly, the septin-bundling activity of Syp1 resides mainly in its intrinsically disordered region. Our data uncover the mechanism through which Syp1 promotes septin collar assembly and offer another example of functional diversity of unstructured protein domains.

INTRODUCTION

Septins are cytoskeletal proteins, first discovered in budding yeast[1] and later found ubiquitously in animal cells and fungi (reviewed in Auxier et al.[2]). Septins form filamentous supra-molecular structures (e.g., arcs or rings) that localize at cellular protrusions, such as the base of cilia and dendritic spines, the annulus of sperm tails, and the bud neck of budding yeast cells.[3] At these locations, septins can act as scaffolds to organize macromolecular assemblies, and as membrane diffusion barriers to dictate subcellular compartmentalization (reviewed in Mostowy and Cossart[4]).
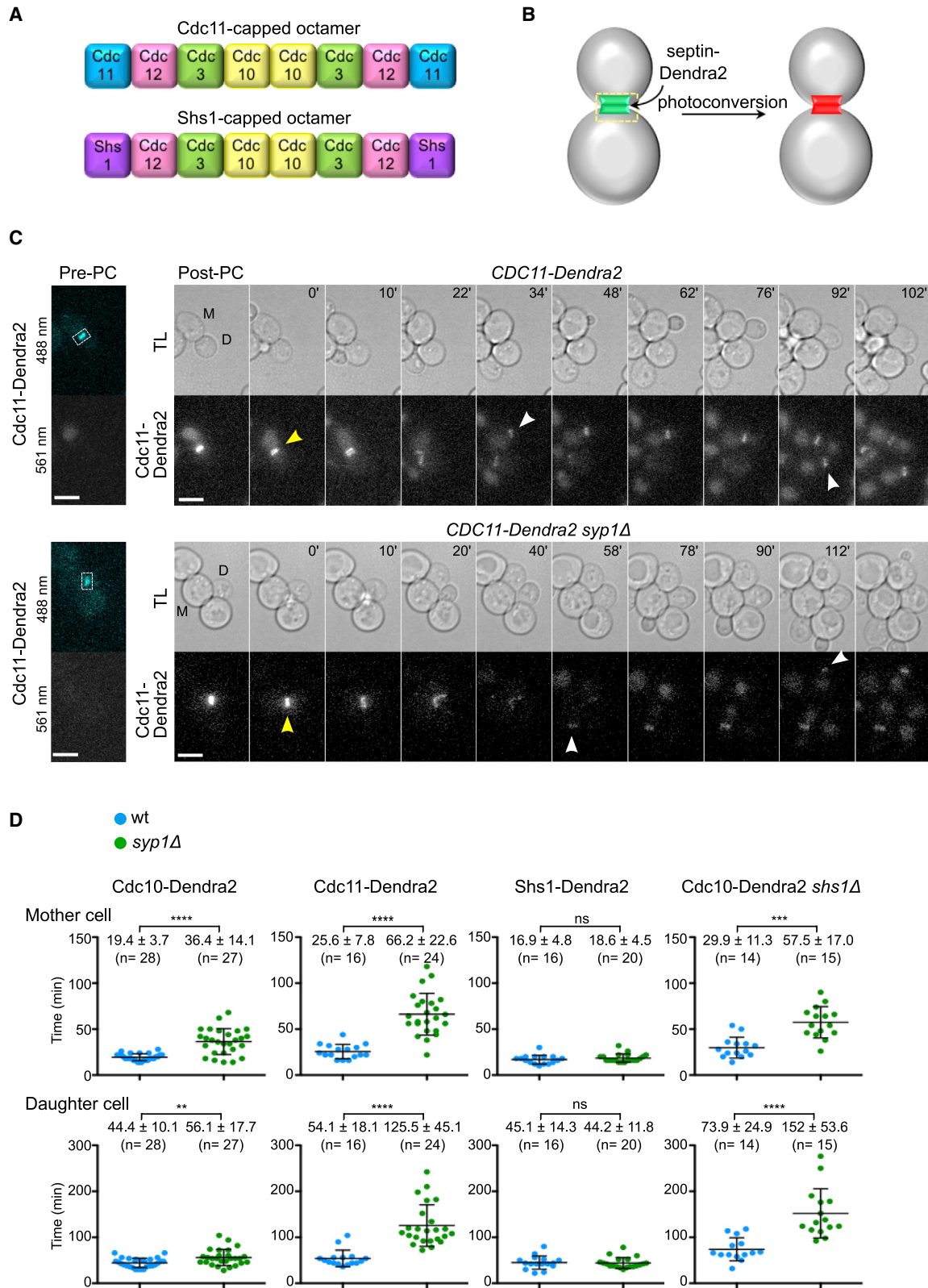
A major function of septins is to promote cytokinesis, the last step of cell division. Septins are strictly required for the organization of the cytokinetic apparatus in budding yeast (reviewed in Bhavsar-Jog and Bi[5] and Juanes and Piatti[6]). Furthermore, they stabilize the contractile actomyosin ring at the cleavage furrow in *Drosophila*[7] and prompt the assembly of the abscission

machinery in mammalian cells.[8] The cytokinetic function of septins is linked to their intimate connection with the plasma membrane (reviewed in Bridges and Gladfelter[9] and Caudron and Barral[10]), but also to their ability to interact with actin, myosin II, and microtubules (reviewed in Spiliotis and Nakos[11]).

Given the complexity of septin assemblies in living cells, *in vitro* reconstitution assays using recombinant septins have greatly contributed to our understanding of septin biology and organization, revealing for instance the intrinsic ability of septins to polymerize into long paired filaments, either in solution or on membranes.[12–21] Binding of septins to membranes is due to their affinity for negatively charged lipids, with a marked preference for phosphatidylinositol-4,5-bisphosphate (PI(4,5)P2) in the case of yeast septins.[13,20,22]

Septin polymerization into filaments occurs by end-to-end joining of linear heteromeric septin complexes,[12,14] also referred to as septin rods, which are invariably composed of two copies of identical septins arranged in a palindromic fashion to give rise

A

Cdc11-capped octamer

| Cdc 11 | Cdc 12 | Cdc 3 | Cdc 10 | Cdc 10 | Cdc 3 | Cdc 12 | Cdc 11 |

Shs1-capped octamer

| Shs 1 | Cdc 12 | Cdc 3 | Cdc 10 | Cdc 10 | Cdc 3 | Cdc 12 | Shs 1 |

B

septin-Dendra2
photoconversion

C

CDC11-Dendra2

CDC11-Dendra2 syp1Δ

D

● wt
● *syp1Δ*

(legend on next page)

to octamers, hexamers, or tetramers depending on the organism and tissue (reviewed in Valadares et al.[23] and Weirich et al.[24]). Two main septin complexes are thought to be present in actively dividing budding yeast cells: Cdc11-capped octamers (Cdc11-Cdc12-Cdc3-Cdc10-Cdc10-Cdc3-Cdc12-Cdc11) and Shs1-capped octamers (Shs1-Cdc12-Cdc3-Cdc10-Cdc10-Cdc3-Cdc12-Shs1)[12,25] (Figure 1A). Since Shs1 is dispensable for cell viability,[25,26] Cdc11-capped octamers may be sufficient for the essential functions of septins in cytokinesis, at least under laboratory growth conditions. In addition, the ability of Cdc11-capped octamers to polymerize into filaments is necessary for cytokinesis.[27] Current models envisage that different kinds of septin filaments build the septin collar at the yeast bud neck, i.e., the structure that scaffolds the cytokinetic machinery at the division site.[28–33] Axial filaments running along the mother-bud axis are intersected by circumferential filaments oriented perpendicularly, to form a rigid, hourglass-shaped gauze (reviewed in Marquardt et al.[34]).

The first step toward the assembly of a mature septin hourglass during the cell cycle is septin recruitment to the presumptive bud site, which occurs in G1 and requires cell polarization by the Cdc42 GTPase.[35–38] At this location septins rapidly organize into a ring and, slightly later, into the mature hourglass, presumably aided by septin-interacting proteins. Immediately prior to cytokinesis, the septin collar splits into two separate rings that sandwich the cytokinetic machinery.[39–41] This transition is essential for actomyosin ring constriction and, ultimately, for cytokinesis.[42]

Many yeast proteins have been identified as septin interactors and/or regulators, yet their specific function in septin architecture and dynamics has been defined only for a limited number of them (e.g., Gic1, Elm1, and Bni5).[43–46]

Here we describe the function of Syp1 in septin organization. Syp1, the yeast homolog of mammalian FCHo1/2, is an endocytic protein of the F-BAR family[47–50] that was also found to interact with septins and facilitate septin ring formation in late G1.[51–54] The precise mechanism underlying the involvement of Syp1 in septin architecture remained to be defined and is the focus of this study.

RESULTS

Syp1 contributes to the recycling of Cdc11-capped septin octamers at the bud neck

Syp1 is required for timely septin recruitment to the presumptive bud site.[51,52] Since septins are recycled from one cell cycle to the next,[53] in order to get precise measurements of Syp1 contribution to septin recruitment, we tracked individual septins during their recycling from split septin rings at the end of mitosis into new septin structures that assemble in the following cell cycle. To this purpose, we individually tagged three septins (Cdc10, Cdc11, and Shs1) at their C terminus with a flexible 6-glycine linker followed by photoconvertible Dendra2, which switches from a green to a red fluorescent form upon brief illumination with 405 nm UV light (Figure 1B). Dendra2 tagging of the three septins under scrutiny did not impair the morphology or proliferation capacity of yeast cells (Figures S1A and S1B), suggesting that it does not perturb septin function. We then photoconverted septin collars in either wild-type or *syp1Δ* cells, and measured in the red channel (561 nm) the time occurring between septin ring splitting and re-appearance of a given septin at the presumptive bud site in the mother and in the daughter cell (Figures 1C and 1D). The three septins were recycled with similar timing (Figure 1D), consistent with the conclusion that Dendra2 tagging does not perturb their incorporation into septin assemblies. Mother cells recycled septins into new rings faster than daughter cells (Figures 1C and 1D), in line with their ability to undergo swifter polarization in G1 relative to daughters.[54] Intriguingly, *SYP1* deletion slowed down the incorporation into new rings of Cdc10 and, even more, of Cdc11 in both mother and daughter cells, while it had no effect on Shs1 recycling Figure 1D). Since Cdc10 is part of both Cdc11- and Shs1-capped septin octamers, we then deleted *SHS1* in wild-type and *syp1Δ* strains to measure the kinetics of Cdc10 recycling in cells bearing only Cdc11-capped septin complexes. Under these conditions, Cdc10 recycling in the absence of Syp1 was further slowed down to kinetics similar to those of Cdc11 (Figure 1D), indicating that Syp1 specifically facilitates the recycling and the incorporation into new rings of septin complexes/filaments bearing Cdc11 at their ends.

Syp1 induces septin filament bundling

The data above, together with the ability of Syp1 to interact and colocalize with septins,[51,52,55] suggest that Syp1 may contribute to shape septin architecture in G1. In order to assess if Syp1 contributes directly to septin organization, we set up *in vitro* reconstitution assays using recombinant Syp1[49] and Cdc11-capped septin octamers.[15] Septin octamers were shortly let to polymerize by lowering the salt concentration (from 300 mM to 30 mM NaCl), in the presence or absence of different molar ratios of Syp1, followed by negative staining and visualization by transmission electron microscopy (TEM). Septin complexes in high salt buffer did not polymerize, while in low salt buffer they readily polymerized into long and often paired filaments (Figure 2A), consistent with previous data.[12] Strikingly, addition of Syp1 during polymerization (septin:Syp1 molar ratios 1:1, 1:0.5 and

Figure 1. Syp1 favors the incorporation of Cdc11-capped septin complexes into newly forming septin rings

(A) Schematic representation of budding yeast Cdc11-capped and Shs1-capped septin octamers.

(B) Depiction of photoconversion of a Dendra2-tagged septin at the yeast bud neck.

(C and D) Wild-type (wt) and *syp1Δ* cells expressing the indicated Dendra2-tagged septin were subject to photoconversion and filmed upon laser illumination at 561 nm. The time occurring between septin ring splitting (i.e., cytokinesis) and appearance of the photoconverted septin into a new septin ring in either the mother or the daughter cell was recorded and plotted in (D). Representative frames of wild-type and *syp1Δ* cells after photoconversion of Cdc11-Dendra2 are shown in (C) as an example. Yellow arrowheads indicate septin ring splitting, while white arrowheads indicate the appearance of a new septin ring in the mother (M) and the daughter cell (D). Post-PC, after photoconversion; Pre-PC, before photoconversion; TL, transmitted light. Statistical differences were assessed by Mann-Whitney *U* test: **p ≤ 0.01; ***p ≤ 0.001; ****p ≤ 0.0001. See also Figure S1.
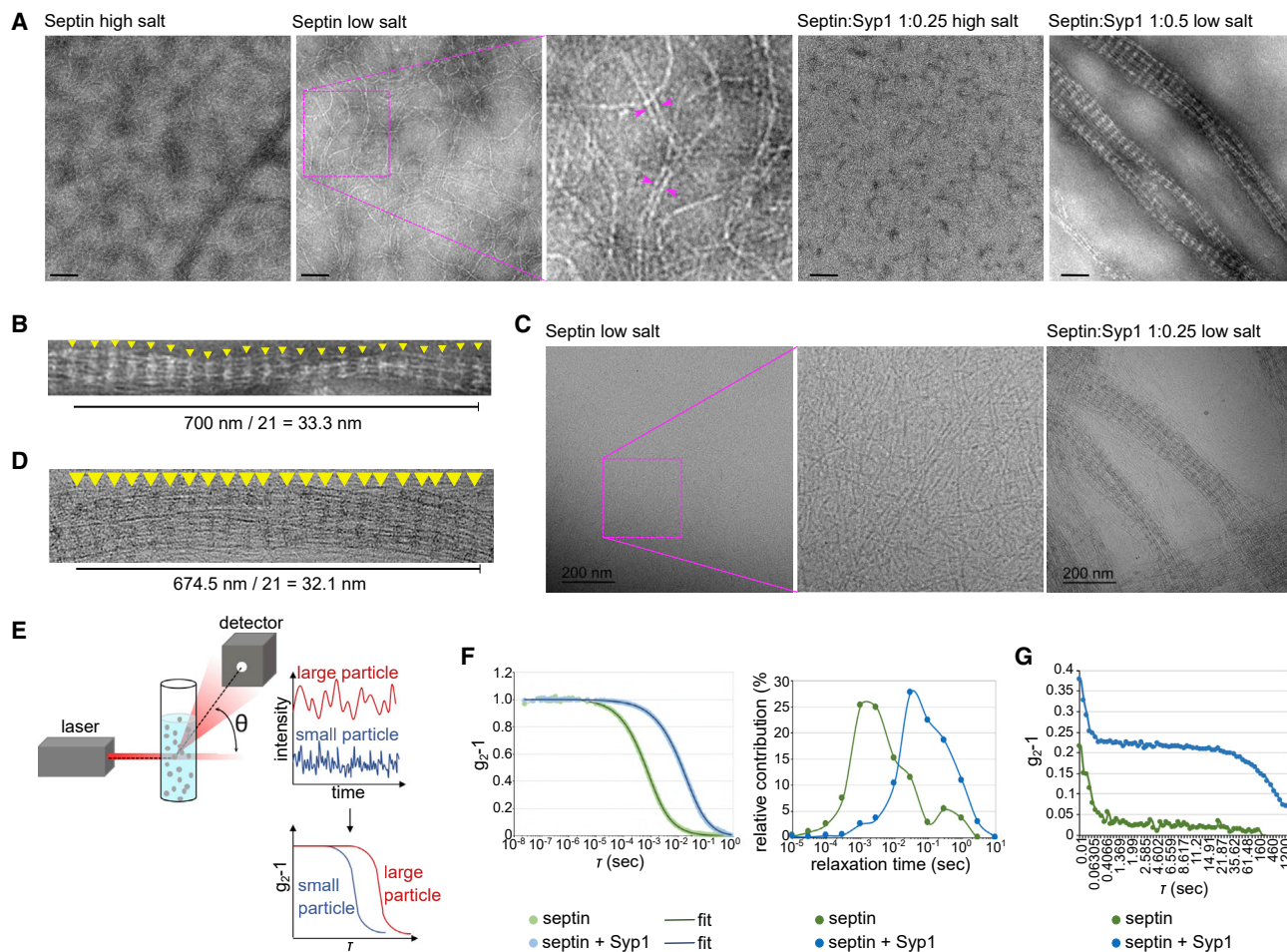
Figure 2. Syp1 bundles Cdc11-capped septin filaments

(A–D) Recombinant Cdc11-capped septin octamers were polymerized in solution in the absence or presence of recombinant Syp1 (ratio septin:Syp1 1:0.25 or 1:0.5). Negatively stained (A and B) or frozen-hydrated (C and D) samples were imaged by transmission electron microscopy. Proteins appear white when they are negatively stained and they appear black in cryo-EM. Scale bar (A), 100 nm. Scale bar (C), 200 nm. Yellow arrowheads in (B) and (D) mark the regular striations whose interval corresponds approximately to the length of a septin octamer (∼32 nm).

(E) Schematic representation of dynamic light scattering (DLS) and image processing.

(F and G) Recombinant Cdc11-capped octamers were polymerized in solution in the absence or presence of Syp1 (ratio septin:Syp1 1:0.5) and analyzed by conventional (F) or multi-speckle (G) DLS, both at a scattering angle of 90°. The intensity correlation function g_2-1 is plotted as a function of the lag time (τ) (F left and G). The lines in (F) are fit to the data with an expression that accounts for a distribution of relaxation modes with different time scales (see STAR Methods). The relative weight of 13 different relaxation times (chosen to be equally spaced in a logarithmic scale, ranging from 10^{-5} to 10 s) is plotted as a function of the relaxation time (F: righthand graph). See also Figure S2.

1:0.25) induced the formation of large bundles made of multiple septin filaments with periodic orthogonal striations (Figures 2A and S2A). The average distance between striations was 33.3 nm (Figure 2B), which roughly corresponds to the long dimension of Cdc11-capped septin rods (32–35 nm[12]), suggesting that septin filaments are in register and presumably undergo homotypic lateral interactions that align identical subunits across a bundle.[12]

To circumvent possible artifacts due to staining required for TEM, we aimed at confirming these results by cryo-electron microscopy (cryo-EM). In agreement with the TEM data, sub-molar ratios of Syp1 induced septin bundling of Cdc11-capped filaments also in this experimental set-up (Figures 2C and S2B),

with bundles displaying lateral banding of about 32 nm periodicity (Figure 2D). The width of Syp1-induced septin bundles was variable and sometime comprised tens of filaments (Figure S2C). In addition, adjacent septin bundles with different orientations could get superimposed to form gauze-like structures (Figure S2C).

In order to obtain a quantitative assessment of Syp1-induced septin bundling, we used dynamic light scattering (DLS, Figure 2E), which allows to obtain information about particle size in solution based on their Brownian motion. The sample is illuminated by a laser, and particle motion is inferred from the temporal fluctuations of the light scattered at a well-defined angle (here 90°), the fluctuations being quantified by the decay time of the
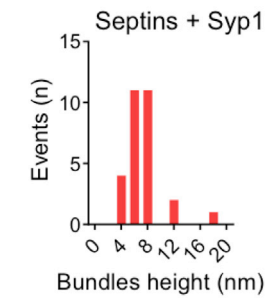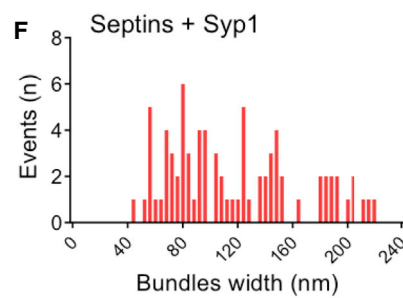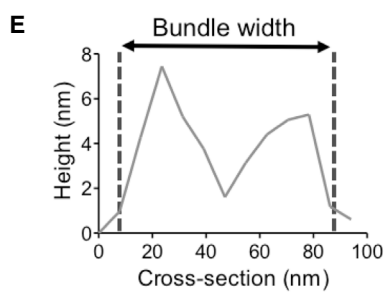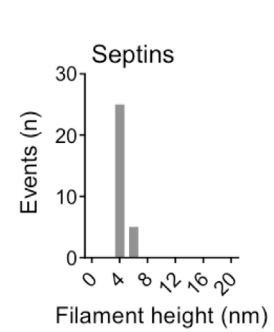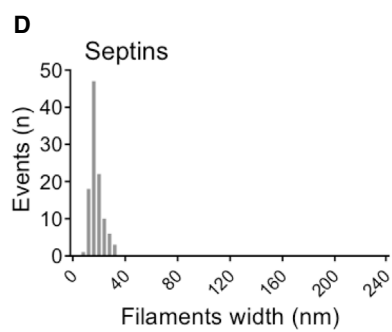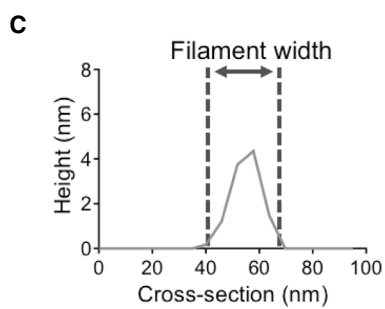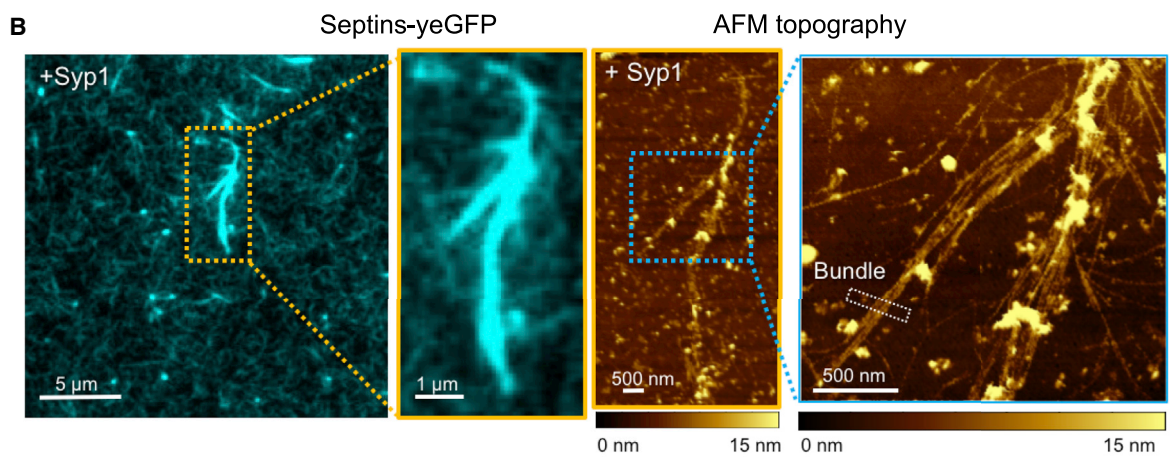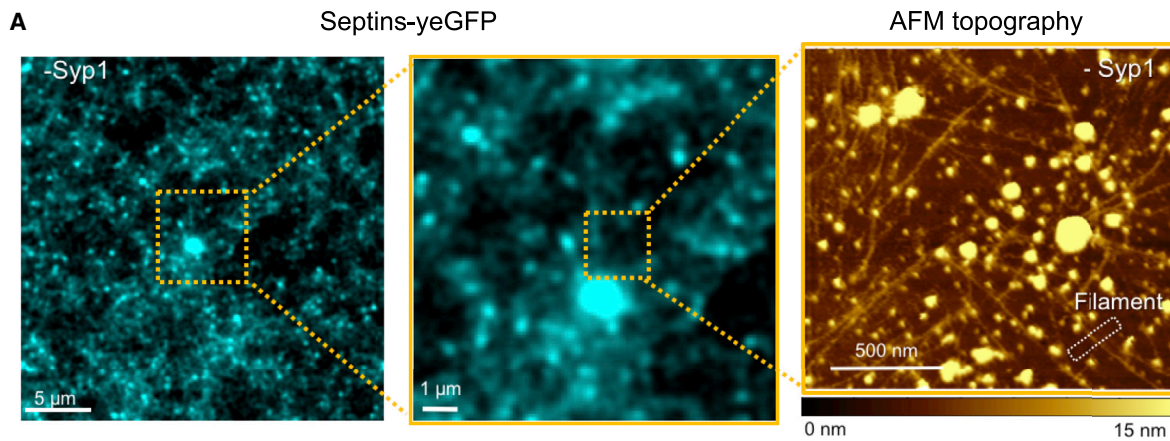
intensity correlation function g_2-1.[56] Smaller particles undergo Brownian motion faster that larger ones, which results in a faster decay of g_2-1 (Figure 2E). Recombinant septin octamers were polymerized in low salt buffer in the presence or absence of Syp1. Intensity correlation functions collected with a conventional DLS set-up exhibited a rather stretched relaxation, incompatible with small, monodispersed particles (Figure 2F, left), suggesting a broad spectrum of relaxation times. To quantify the distribution of relaxation times, we fitted the data with the sum of exponentially relaxing modes. We found that an excellent fit was obtained using 13 modes with characteristic times chosen to be equally spaced in a logarithmic scale, ranging from 10^{-5} to 10 s (Figure 2F, right). This indicates significant polydispersity of both protein samples and suggests a wide range of particle sizes, as typically observed in aggregating systems. Crucially, the distribution of relaxation times was shifted to values 20- to 30-fold higher when septins polymerized in the presence rather than in the absence of Syp1 (Figure 2F, right), consistent with the propensity of septin filaments to bundle in the presence of Syp1.

To further investigate the tendency of septins to form aggregates, we used a custom multi-speckle DLS set-up suited to study slow dynamics. In this case, we recorded data during longer incubation times, which allowed us to probe the long-term aggregation behavior. For both conditions (septins alone or septins + Syp1), g_2-1 exhibited a two-step decay, the first decay occurring at time scales ~0.01 s, barely accessible to this set-up (Figure 2G). For septin complexes alone, the initial decay relaxed almost completely g_2-1. By contrast, in the presence of Syp1 an intermediate plateau was clearly apparent, followed by a relaxation at time scales of 1,000 s or higher. Both the intermediate plateau and the ultra-slow relaxation are hallmarks of gel systems,[57] indicating that Syp1 promotes strong aggregation of septin filaments, eventually resulting in gel-like assemblies.

We then characterized the structural organization of septin bundles by atomic force microscopy (AFM). Fluorescent septin octamers that included Cdc3-yeGFP were allowed to polymerize in solution in the absence or presence of half-molar amounts of Syp1 and injected onto supported lipid bilayers made of 95.8% DOPC (mol %) and 4% DGS-NTA(Ni), to which septins bound by virtue of the hexahistidine tag on Cdc3. Trace amounts (0.2%) of rhodamine-labeled phosphatidylethanolamine were included in the lipid mixture to assess the quality and homogeneity of the bilayers. In agreement with previous experiments, AFM topography images showed sparsely distributed septin filaments in the absence of Syp1 (Figure 3A) and thick septin bundles in its

presence (Figure 3B). The width of septin filaments in the absence of Syp1 ranged from 8 to 32 nm (Figures 3C and 3D), suggesting that they are mostly paired filaments with different degrees of inter-filament spacing.[12,13] In contrast, septin bundles assembled in the presence of Syp1 displayed a wide distribution of widths, ranging from 40 to 280 nm (Figures 3E and 3F), which is compatible with up to several tens of septin filaments aligned laterally and tightly packed.

The height of septin filaments was quite uniform and peaked at 4 nm (Figures 3C and 3D), which reflects the diameter of the yeast septin rod.[12] In contrast, the height of septin bundles was mostly around 6 to 8 nm (Figures 3E and 3F), suggesting that they might contain two layers of packed filaments stacked on top of each other. Alternatively, the higher height of Syp1-mediated bundles relative to filaments may depend on Syp1 itself (see below). In any case, the narrow distribution of heights indicates that bundles are mostly mono- or double-layered.

Finally, we asked if Syp1 is itself part of septin bundles. To this end, we purified recombinant Syp1 tagged at the C terminus with BFP and used it to study its possible co-localization with septin bundles. Since preliminary experiments showed that BFP tagging of Syp1 interfered with its septin-bundling activity (data not shown), we used it mixed to untagged Syp1 at 1:1 molar ratio. Cdc11-capped yeGFP-tagged yeast septin octamers were let to polymerize in the presence of half-molar amounts of Syp1 (septin:Syp1:Syp1-BFP molar ratio 1:0.25:0.25) in low salt buffer (30 mM) and then injected onto supported lipid bilayers containing 4% (mol %) DGS-NTA(Ni). Imaging by sub-diffracted Airyscan microscopy showed a high degree of Syp1 co-localization with septin bundles, but not with septin filaments in the background (Figures 4A–4C), indicating that Syp1 not only induces septin bundles but it is integral part of them.

The intrinsically disordered domain of Syp1 is the main determinant of septin bundling

Syp1 has an F-BAR domain at the N terminus that clusters phospholipids and induces membrane curvature, a large region predicted to be intrinsically disordered in the middle and a Mu-homology (μHD) domain at the C terminus that mediates its interaction with endocytic proteins and cargos[47,49,58] (Figures 5A and 5B). In order to map the domain responsible for septin bundling, we purified individually from bacteria the three domains described above (F-BAR: aa 1–264; middle region: aa 265–565; μHD: aa 566–870).[49] Characterization of their secondary structures has been performed by circular dichroism (CD) (Figure S3). As predicted by the Alphafold model of Syp1 3D-structure (Figure 5B), CD confirmed that the F-BAR domain was

Figure 3. AFM imaging of Syp1-induced septin bundles

(A and B) Correlative fluorescence (left) and AFM topography (right) images of membrane-bound septin-yeGFP filaments formed at a low salt concentration (30 mM NaCl) on lipid bilayers containing 95.8% mol DOPC, 4% mol DGS-NTA(Ni), and 0.2% mol Rhodamin-PE in the absence (A) or presence (B) of Syp1. Magnified fluorescence and AFM topography images correspond to the dashed boxes. The false-color scale is 15 nm. Scale bar is 500 nm for AFM topography and 5 μm for fluorescence images or 1 μm for the magnified region.

(C and E) Representative cross-section analysis corresponding to the white dashed boxes in the righthand images in (A) and (B) showing the width of septin filaments (C) and bundles (E).

(D and F) Frequency distribution of septin filament widths and heights in the absence (D) or in the presence (F) of Syp1. The number of septin assemblies (n) analyzed per condition were n = 107 (width) and n = 30 (height) in the absence of Syp1; n = 81 (width) and n = 29 (height) in the presence of Syp1, from three technical replicates.
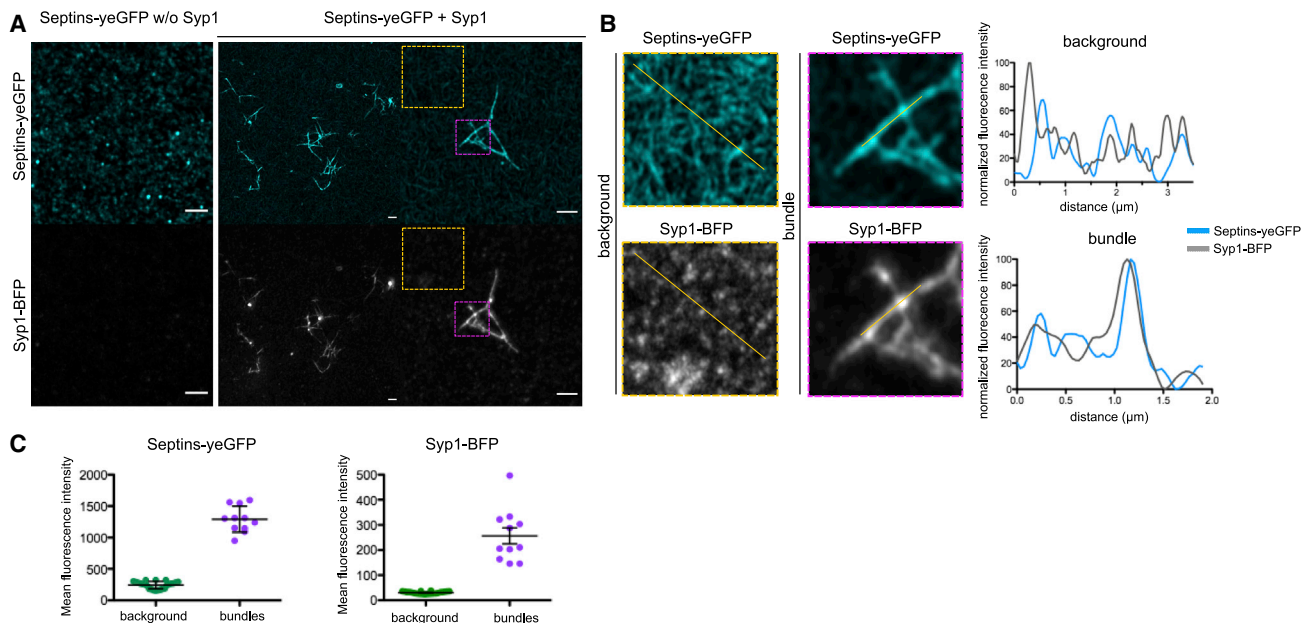
Figure 4. Syp1 is part of the septin bundles
(A–C) yeGFP-tagged septin octamers were polymerized in solution in the presence of untagged and BFP-tagged Syp1 (ratio septins-yeGFP:Syp1:Syp1-BFP 1:0.25:0.25) and deposited onto supported lipid bilayers for imaging by sub-diffraction fluorescence microscopy. Representative images are shown in (A). Scale bar, 2 μm. Selected regions in (A) corresponding to septin filaments in the background (yellow dashed box) and to a septin bundle (magenta dashed box) are magnified in (B) for both channels (septin-yeGFP and Syp1-BFP). Brightness and contrast have been increased for the background insets in (B) relative to (A) for better visualization of septin filaments. Linescan plotting of fluorescent signals along the background and the bundle (yellow lines in B) are shown in the righthand graphs. Note the high and low correlation of signal intensities between Syp1-BFB and septins-yeGFP in the bundle and background, respectively. (C) Distribution of mean fluorescence intensities corresponding to either the background of septin filaments or the bundles has been plotted for both channels (septin-yeGFP and Syp1-BFP). n = 24 for background and n = 12 for bundles.

completely structured, with 100% of α-helices along its length, while the μHD domain was mainly composed by β-sheets (∼70%) and, to a minor extent, by α-helices (∼10%–15%) and random coils (∼20%) (Figure S3). The middle domain showed a markedly different CD spectrum compared with the other two domains, with approximately 70% of unstructured primary sequence and 30% of residues organized as α-helices, more specifically as 3_{10} helices (Figure S3). This secondary structure distribution indicates a largely disordered domain, in agreement with the predictions.

We then tested the ability of these truncated proteins to induce septin bundling *in vitro* in low salt buffer. Recombinant full-length Syp1 or truncated proteins were mixed with yeGFP-tagged septin octamers and shortly let to polymerize in low salt buffer before deposition on supported lipid bilayers. In agreement with our electron microscopy data, full-length Syp1 induced thick and highly fluorescent bundles, while evenly distributed septin filaments were visible in the background (Figure 5C left images and quantification of the background pixel intensity on the right). For what concerns the individual Syp1 protein domains, septin filament bundling was observed only in the presence of the central disordered domain of Syp1, while the F-BAR and the μHD domain did not induce bundling on their own (Figure 5C). These results paralleled the levels of fluorescence associated to the randomly distributed unbundled septin filaments on the supported lipid bilayers (background), which were higher in the pres-

ence of the F-BAR or μHD domain than with the middle region (Figure 5C). We noticed that the middle region of Syp1 led to somewhat looser bundles with lower fluorescence intensity compared with those induced by the full-length protein (Figure 5D), suggesting that septin filaments might be fewer and/or less compactly aligned. Therefore, the F-BAR and/or the μHD domain may contribute to bundling, even though they are insufficient on their own.

We confirmed these results by TEM after negative staining of septin filaments polymerized in solution at low salt concentrations in the presence of different parts of Syp1. Only Syp1 middle region, but neither the F-BAR nor the μHD domain, could bundle septin filaments under these conditions (Figure 5E). It should be noticed, however, that septin bundles induced by the middle unstructured region of Syp1 differed from those obtained with full-length Syp1 in that they lacked periodic banding, again suggesting that the F-BAR and/or the μHD contribute to the spatial alignment of septin filaments within bundles. We therefore repeated the septin polymerization assays with recombinant Syp1 proteins that spanned either the F-BAR and middle domain (aa 1–565) or middle region and μHD (aa 265–870). Remarkably, addition of the F-BAR + middle region induced septin filament bundling with periodic orthogonal striations (Figure 5F), thus fully recapitulating the behavior of full-length Syp1. In stark contrast, the presence of the μHD domain abolished the ability of the central region to promote septin bundling (Figure 5F). The reason for
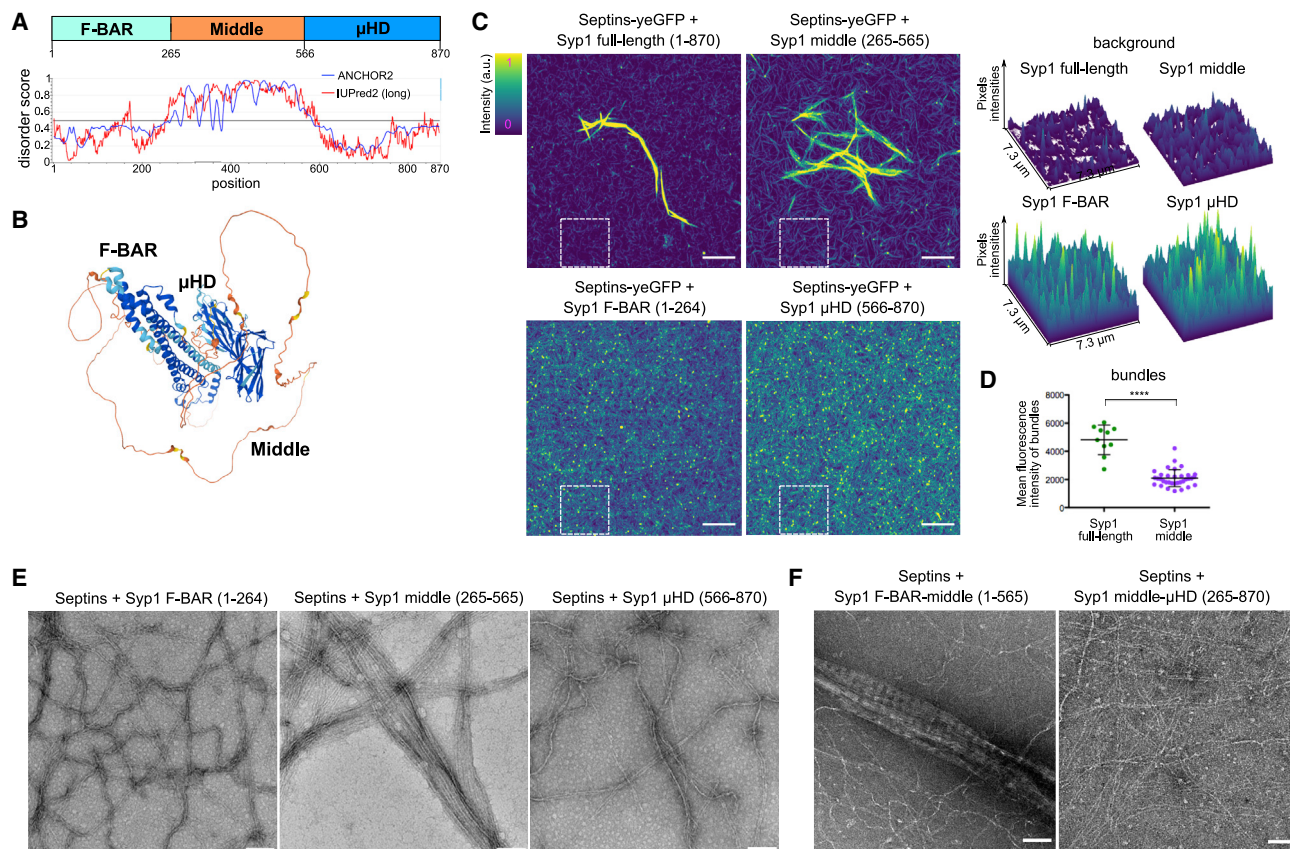
Figure 5. The middle unstructured domain of Syp1 is responsible for septin filament bundling

(A) Top: Schematic view of Syp1 domain organization. Bottom: IUPred2 prediction of domain disorder (IUPred2, red curve) and protein binding regions in disordered domains (ANCHOR2, blue curve).[59] The score indicates the probability of each residue to be part of a disordered domain.

(B) Alphafold model of Syp1 3D-structure showing the structured F-BAR and µHD domains (in blue) and the middle unstructured region (in yellow/orange).

(C and D) yeGFP-tagged septin octamers were polymerized in the presence of full-length Syp1 (ratio septins:Syp1 1:0.5), F-BAR domain (aa 1-264; ratio septins:Syp1(1–264) 1:0.5), middle region (aa 265–565; ratio septins:Syp1(265–565) 1:0.5) or µHD domain (aa 566–870; ratio septins:Syp1(566–870) 1:0.5) and injected onto supported lipid bilayers for sub-diffraction fluorescence imaging. Representative images are shown in (C). Scale bar, 5 µm. Fluorescence intensities of sparse septin filaments on the lipid bilayers (background) were measured within the dashed white boxes and plotted in the righthand plots. The intensity scale is shown on the top left. Fluorescence intensities of bundles assembled in the presence of full-length Syp1 or its middle unstructured domain were measured using the Analyze Particle tool of Fiji after appropriate thresholding of fluorescent signals. Mean intensities of bundles was plotted in (D). n = 10 for full-length Syp1 and n = 34 for Syp1 middle region. Statistical differences were assessed by Mann-Whitney U test: ****p $\leq$ 0.0001.

(E and F) Cdc11-capped septin octamers were polymerized as in (C) in the presence of the indicated Syp1 protein domains (ratio septins:Syp1(1–264) 1:0.5; septins:Syp1(265–565) 1:0.25; septins:Syp1(565–870) 1:0.5; septins:Syp1(1–565) 1:0.5; septins:Syp1(265–870) 1:0.5). Samples were negatively stained for visualization by transmission electron microscopy. Scale bar, 100 nm. See also Figure S3.

this is presently unclear, but we hypothesize that either the protein is improperly folded or the µHD domain has an inhibitory effect on septin bundling that is obliterated in the full-length protein.

Altogether, these results highlight the central disordered domain of Syp1 as the main determinant of Syp1-mediated septin bundling. The F-BAR domain contributes to the lateral alignment of septin filaments and to bundle compaction.

The mammalian muniscin FCHo2, but not an unrelated intrinsically disordered protein, is able to promote bundling of yeast septin filaments

To investigate if the septin-bundling properties of Syp1 are conserved throughout evolution, we carried out *in vitro* septin

polymerization assays in the presence of the mouse endocytic adaptor FCHo2, which shares a similar structural organization with Syp1, bearing an N-terminal F-BAR domain, a C-terminal µHD domain and a middle intrinsically disordered region (Figures 6A and 6B).[49] Due to their common structural organization, these proteins have been collectively named muniscins.[49] While the disordered domains of Syp1 and FCHo2 have similar length, they share low sequence similarity (<20% amino acid identity) and have different isoelectric point (8.65 for Syp1 and 6.45 for FCHo2). Fluorescent yeast septin octamers were polymerized in low salt buffer (30 mM NaCl) in the absence or presence of increasing molar amounts of FCHo2 and deposited on supported lipid bilayers. Interestingly, FCHo2 could readily induce the formation of long and thick septin bundles at all
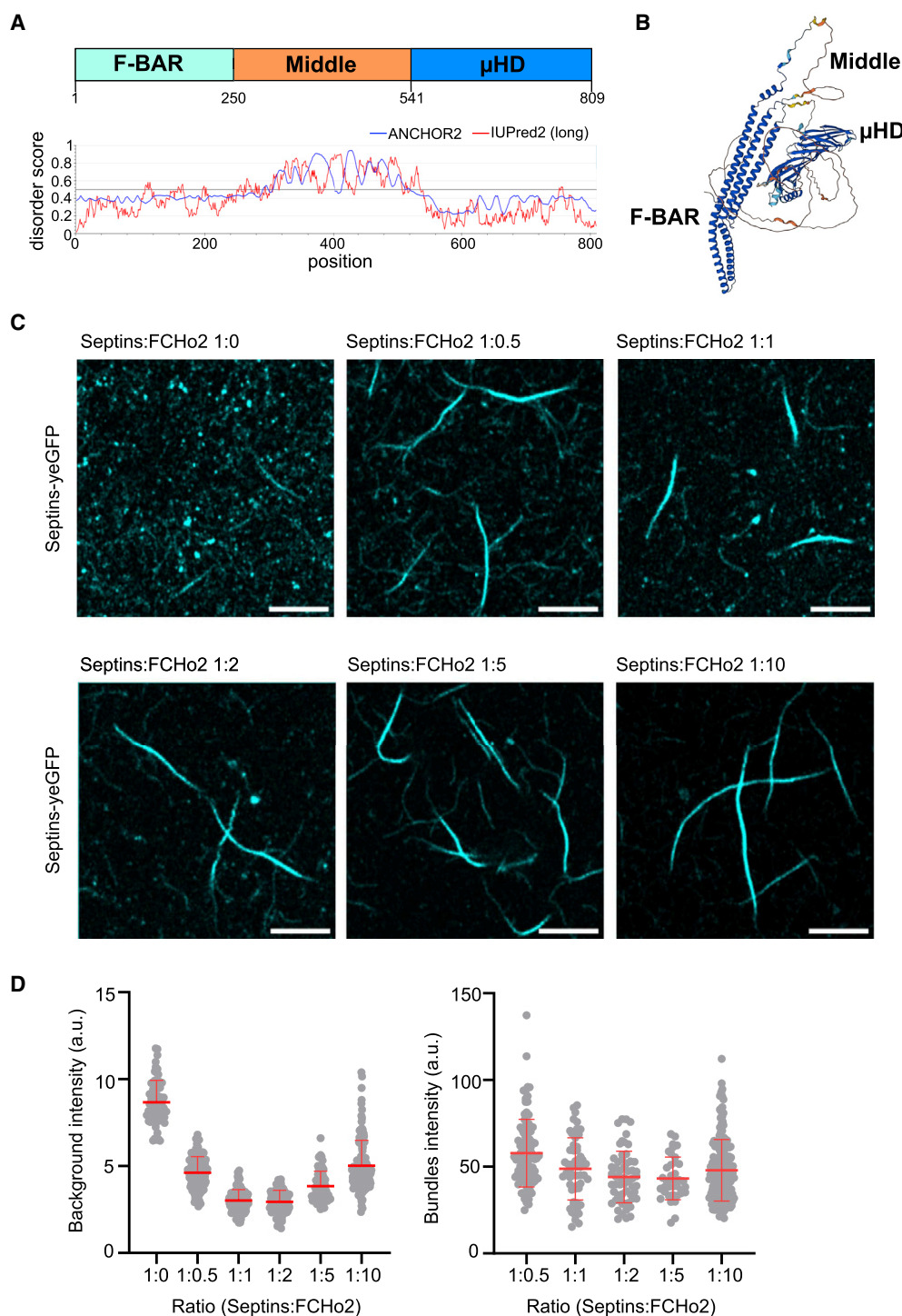
Figure 6. Mammalian FCHo2 induces yeast septin filament bundling

(A) Top: Schematic view of mouse FCHo2 domain organization. Bottom: IUPred2 prediction of domain disorder (IUPred2, red curve) and disordered protein binding regions (ANCHOR2, blue curve).

(B) Alphafold model of mouse FCHo2 3D-structure showing the structured F-BAR and µHD domains (in blue) and the middle unstructured region (in yellow/orange).

(C) yeGFP-tagged septin octamers (cyan) were polymerized in low salt buffer in the absence (ratio septins:FCHo2 1:0) or presence of unlabeled full-length FCHo2 (ratio septins:FCHo2 was 1:0.5, 1:1, 1:2, 1:5, and 1:10). Samples were then injected onto supported lipid bilayers for sub-diffraction fluorescence imaging. Scale bar, 5 µm.

(legend continued on next page)

concentrations tested (Figure 6C). Fluorescence intensities of septin-yeGFP in the bundles were several folds higher than in the sparsely distributed filaments (background) and did not increase with FCHo2 concentration (Figure 6D). In addition, fluorescence associated to septin filaments in the background diminished in the presence of FCHo2 (Figure 6D), in agreement with their recruitment into bundles. Collectively, these data suggest that the septin-bundling function of muniscins may be evolutionarily conserved. However, properties other than the primary sequence of their intrinsically disordered domains likely underlie their ability to organize septin filaments.

To address if the ability to promote septin bundling is a common feature of disordered proteins, we repeated the *in vitro* septin polymerization assays in the presence of Nab3, an RNA-binding protein that is predicted to be largely unstructured (Figures S4A and S4B). Nab3 was previously shown to form granules in yeast cells and amyloid-like fibers *in vitro* that depend on its low complexity prion-like domain.[60,61] Cdc11-capped octamers were polymerized in low salt buffer (30 mM) in the presence various molar ratios of Nab3 (1:0, 1:0.25, 1:0.5 and 1.1). Visualization of septin structures by TEM after negative staining (Figure S4C) showed that paired septin filaments, but not bundles, were visible both in the absence and in the presence of Nab3, suggesting that septin bundling is not an aspecific property of intrinsically disordered proteins.
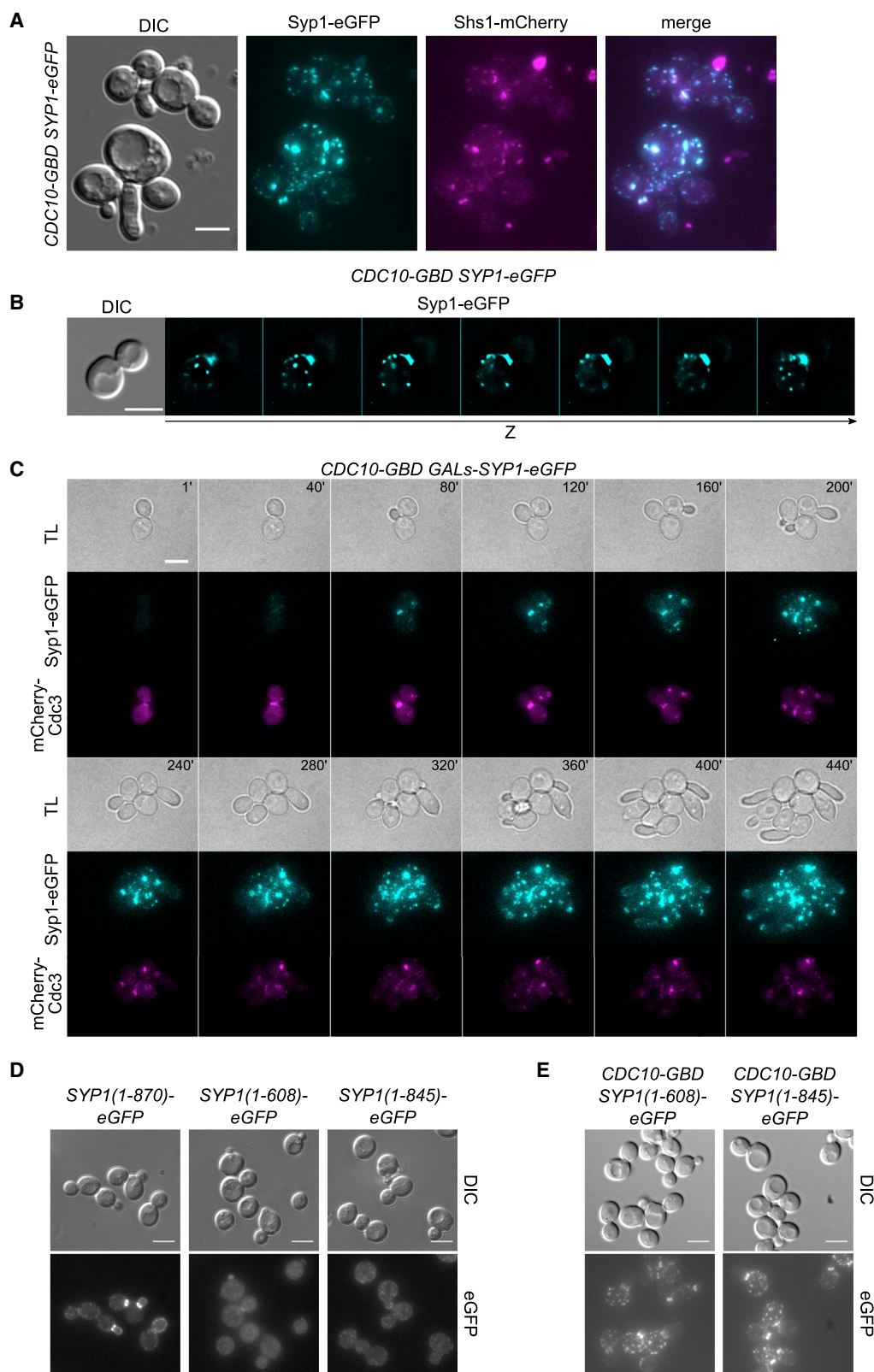
Constitutive binding of Syp1 to septins *in vivo* causes ectopic septin bundling at the plasma membrane and morphological defects

Syp1 binding to septins is likely to be tightly regulated in yeast cells, to avoid interfering with the changes in septin dynamics that accompany cell cycle transitions.[35,62] Consistently, Syp1 overexpression leads to septin disorganization.[52] Syp1 was shown to co-purify with septins in telophase-arrested cells[55] and to interact with septins in two-hybrid assays[52] and protein-fragment complementation assays.[63] Despite our efforts, we have been unable to detect Syp1 in septin immunoprecipitations from yeast extracts or reconstitute Syp1-septin interaction through a tripartite GFP system,[64,65] suggesting that Syp1 association to septins *in vivo* might be highly dynamic.

To study the consequences of constitutive Syp1 binding to septins in yeast cells, we tagged the septin Cdc10 with a GFP-nanotrap (GFP-binding domain or GBD)[66] in cells that expressed at the same time Syp1-eGFP. This led to Syp1-eGFP localizing to the bud neck, as well as to ectopic clusters that mostly co-localized with the septin Shs1-mCherry and likely correspond to septin bundles (Figure 7A). The ectopic Syp1-septin clusters were almost exclusively found in the mother cell compartment (Video S1), consistent with the preferential localization of Syp1 at the mother-side of the septin collar.[51] In addition, clusters were relatively immobile and mostly localized at the cortex (Figure 7B), although some mobile, cytoplasmic clusters were occasionally apparent. A fraction of cells were abnormally shaped and usually

displayed low levels of Shs1-mCherry at the bud neck (Figure 7A), suggesting that septin cluster formation occurs at the expenses of the septin collar. However, we noticed that *CDC10-GBD SYP1-eGFP* strains freshly generated by crossing and sporulation were initially very sick, but became progressively healthier within a few cell divisions, suggesting that they are able to adapt to this unphysiological condition. To overcome this problem, we generated an inducible system where Syp1-eGFP expression was driven by the attenuated galactose-inducible *GALs* promoter.[67] Cells were grown in raffinose-containing medium (*GALs-SYP1-eGFP* off) and induced by galactose immediately before live cell imaging. Under these conditions, cells had initially a normal appearance and bore the septin mCherry-Cdc3 at the bud neck, as expected (Figure 7C and Video S2). With time, cells progressively accumulated Syp1-eGFP, both at the bud neck and in ectopic clusters. At later time frames, cells were literally filled with ectopic Syp1-eGFP clusters and exhibited low levels of mCherry-Cdc3 at the bud neck as well as markedly elongated buds, which are typical of cells with septin defects.[68–70] While most Syp1-septin ectopic clusters were associated with the plasma membrane, the presence of large mobile cytoplasmic "aggregates" was more frequent in strains expressing Syp1-eGFP from the *GALs* promoter than from the endogenous *SYP1* promoter. These cytoplasmic aggregates were usually associated with the vacuolar membrane, as revealed by staining with the endomembrane dye FM4-64 (Figures S5A and S5B) and are likely to have a different nature from those at the plasma membrane. Indeed, we could observe them in some, but not all, *GALs-SYP1-eGFP* strains independent of the presence of *CDC10-GBD* (Figures S6A and S6B and Videos S3 and 4). These aggregates are reminiscent of the cytoplasmic droplets arising from liquid-liquid phase separation of Ede1, the endocytic partner of Syp1, as a consequence of endocytic defects or *EDE1* overexpression.[71–73] Consistently, the intrinsically disordered region of Syp1 is predicted to have high propensity to form droplets according to the Fuzdrop software (https://fuzdrop.bio.unipd.it; Figure S6D). Although the significance of these cytoplasmic aggregates remains to be assessed, we note that expression of *GALs-SYP1-eGFP* on its own never led to formation of the ectopic clusters at the mother cell plasma membrane that we observed upon forced interaction between Syp1 and Cdc10. In addition, cells expressing *GALs-SYP1-eGFP* had wild-type morphology, showed unperturbed localization of mCherry Cdc3 at the bud neck and never displayed an elongated bud phenotype (Figures S6A and S6B and Videos S3 and S4). In contrast, we could generate *CDC10-GBD SYP1-eGFP* strains that lacked the cytoplasmic aggregates after galactose induction but still accumulated ectopic clusters on the mother cell plasma membrane and displayed and elongated phenotype (Figure S6C and Video S5), supporting our hypothesis that ectopic membrane-associated clusters deplete septins from the collar at the bud neck and may represent the septin bundles observed *in vitro*.

(D) Distributions of fluorescence intensities of background septin filaments and septin bundles in the absence or presence of different ratios of recombinant FCHo2 measured after appropriate thresholding of fluorescence signals. Mean +SD is shown in red. The number of regions of interest analyzed per condition was n = 69, n = 106, n = 106, n = 91, n = 76, and n = 136 for the background, respectively, and n = 99, n = 57, n = 60, n = 39, and n = 187 for the bundles, respectively. See also Figure S4.

A CDC10-GBD SYP1-eGFP

DIC | Syp1-eGFP | Shs1-mCherry | merge

B CDC10-GBD SYP1-eGFP

DIC | Syp1-eGFP

Z

C CDC10-GBD GALs-SYP1-eGFP

TL | 1' | 40' | 80' | 120' | 160' | 200'

Syp1-eGFP

mCherry-Cdc3

TL | 240' | 280' | 320' | 360' | 400' | 440'

Syp1-eGFP

mCherry-Cdc3

D SYP1(1-870)-eGFP | SYP1(1-608)-eGFP | SYP1(1-845)-eGFP

DIC

eGFP

E CDC10-GBD SYP1(1-608)-eGFP | CDC10-GBD SYP1(1-845)-eGFP

DIC

eGFP

(legend on next page)

Localization of Syp1 at the bud neck requires its μHD domain,[49] which may seem at odds with the conclusion that the disordered region of Syp1 binds to and bundles septin *in vitro*. We confirmed that, while full-length Syp1 robustly accumulated at the bud neck of small- and medium-budded cells (Figure 7D and Video S6), bud neck recruitment of a truncated Syp1 counterpart lacking the μHD domain (Syp1(1-608)) was severely compromised (Figure 7D and Video S7). In addition, a smaller truncation (Syp1(1-845)) that eliminates only the last 25 amino acids at the C terminus carrying the Asn-Pro-Phe (NPF) motif that is predicted to bind Syp1's endocytic partner Ede1[49] also hampered Syp1 localization at the bud neck (Figure 7D and Video S8). We then took advantage of the GBP-GFP strategy described above to force the interaction of these truncated proteins with septins. Remarkably, both Syp1(1-608)-eGFP and Syp1(1-845)-eGFP were now recruited to the bud neck and induced the formation of ectopic septin clusters at the mother cell's plasma membrane in the presence of Cdc10-GBD (Figure 7E), thus supporting the idea that the disordered domain of Syp1 is capable of inducing septin bundling *in vitro* and *in vivo*. In contrast, the μHD domain and the NPF motif may be involved in Syp1 interaction with septins at the bud neck.

DISCUSSION

How septin architecture is tuned by the plethora of septin-binding proteins that exist in living cells is an open question and subject of intense investigation. Here we focused on the role of the Syp1/FCHo2 protein in septin organization and, in particular, on its ability to align and tightly pack septin filaments. Previous data indicated that budding yeast Syp1 is required for proper kinetics of septin ring assembly in late G1, which is consistent with its early recruitment to the presumptive bud site, concomitant to septins.[51,52] Through photoconversion experiments, we find that Syp1 specifically aids the incorporation of Cdc11-capped septin filaments into the newly assembling septin ring in late G1, while it has no apparent effect on the recruitment of Shs1-capped octamers. How this specificity is achieved remains to be investigated, but it is plausible that Syp1 recognizes and binds preformed septin filaments. Indeed, while Cdc11-capped octamers polymerize into filaments by end-to-end joining,[12,14] Shs1-capped octamers do not.[25] In addition, our *in vitro* reconstitution assays show that Syp1 does not prompt the formation of septin bundles in high salt buffer, where septin complexes do not polymerize.[12]

The septin collar is made by an ordered array of axial filaments oriented along the mother-bud axis that are thought to be mainly made by Cdc11-capped octamers, while Shs1-capped septin octamers likely compose and organize the circumferential filaments that intersect orthogonally the axial filaments.[28,31] Since Cdc11-capped septin filaments have a low propensity to bundle spontaneously,[20] it is conceivable that septin-bundling proteins are involved in the alignment and organization of septin filaments along the mother-bud axis, thereby conferring mechanical stability to the collar. Together with its early recruitment to septins, Syp1 is at the right place at the right time to support the orderly integration of septin filaments into the collar. It should be noticed, however, that Syp1 is dispensable for the formation of the septin collar, suggesting that other proteins, yet to be identified, can fulfill this function. Given the essential role of the septin collar in budding yeast cell division, it is not surprising that the assembly of such a crucial cytoskeletal element relies on redundant factors.

Another important conclusion stemming from our data is that the central intrinsically disordered domain of Syp1 is mainly responsible for its septin bundling activity. However, the F-BAR domain contributes, in combination with the middle region, to align septin filaments in register and pack them into tighter bundles.[49,74] It is conceivable that dimerization of the F-BAR domain[49,74] connects laterally the same septin subunits in adjacent filaments, thereby introducing order and compaction. Remarkably, the mammalian protein FCHo2, which has an unstructured domain of similar length as Syp1, as well as a similar structural organization of structured domains, is also able to bundle efficiently yeast septin filaments, suggesting that this function has been conserved throughout evolution.

In general, disordered domains can account for the plasticity of protein structure/function and underlie multi-functionality (referred to as "moonlighting"[75,76]). Indeed, thanks to their conformational freedom, disordered domains can act as flexible linkers between structured domains to diversify the acquisition of supertertiary structures.[77] In addition, because of their enlarged capture radius, disordered domains can bridge large distances via the "fly-casting mechanism" of protein binding, thereby speeding up the assembly of multi-protein complexes.[78,79] Thus, the involvement of Syp1 in diverse processes, such as endocytosis,[48–50] actin remodeling,[48,80] and septin architecture[51,52] (and this manuscript), may reflect the plasticity of its disordered domain. It is therefore not surprising that most of the posttranslational modifications of Syp1, including 40 phosphorylation and five ubiquitylation sites, lie in this region (www.phosphogrid.org).

Although the aforementioned models envision a crucial regulatory role for disordered domains in protein conformation and

Figure 7. Forced interaction between Syp1 and septins is detrimental for the septin collar and cell shape

(A) Still images of cells co-expressing Cdc10-GBD and Syp1-eGFP, as well as Shs1-mCherry. Note the ectopic clusters of Syp1-septins in the mother cells. Scale bar, 5 μm.

(B) z stack images of a representative *CDC10-GBD SYP1-eGFP* cell showing that Syp1-septin clusters are mainly localized at the plasma membrane. Scale bar, 5 μm.

(C) *CDC10-GBD GALs-SYP1-eGFP* cells co-expressing mCherry-Cdc3 were grown at 30°C in raffinose-containing medium (*GALs* promoter off) and induced with galactose (*GALs* promoter on) immediately prior to filming. Note the accumulation of septin-Syp1 clusters and the concomitant depletion of mCherry Cdc3 at the bud neck accompanied by the hyperpolarization of buds. Scale bar, 5 μm.

(D and E) Cells expressing eGFP-tagged truncated versions of Syp1 from its endogenous locus in the absence (D) or in the presence (E) of Cdc10-GBD were imaged by fluorescence microscopy. Scale bars, 5 μm. See also Figures S5 and S6.

interaction of structured domains, we show that the disordered domain of Syp1 alone is sufficient to bundle septins, which is incompatible with the idea that it only acts as a flexible linker. Similarly, the unstructured region of Syp1 was shown to directly inhibit Las17/WASp-dependent actin polymerization by the Arp2/3 complex,[48] suggesting that it has a direct role in its different activities and might serve as a paradigm to expand our knowledge of the complexity and adaptability of disordered regions. Whether upon binding to septins the middle region of Syp1 undergoes a disordered-to-ordered conformational switch, as it was previously shown for other proteins,[81] remains to be established. In addition, since our data indicate that constitutive Syp1-septin association is detrimental for the septin collar, how Syp1 interaction with septins is controlled to preserve the changes in septin dynamics throughout the cell cycle is an important question that deserves future studies.

During clathrin-mediated endocytosis, Syp1/FCHo2 binds to Ede1/Eps15 through its μHD domain to form an initiator complex that recruits downstream proteins to endocytic sites.[50,82–84] FCHo2 and Eps15 were recently shown to form liquid-like assemblies that act as endocytic catalysts. Intriguingly, these liquid-like networks rely on weak interactions and involve the disordered regions of both proteins.[85] Budding yeast Ede1, the endocytic partner of Syp1, was also found to form liquid condensates *in vivo*, which were attributed to an autophagic pathway warranting the quality control of endocytosis[73] or to initiation of endocytic events.[72] We show that Syp1 can form similar cytoplasmic "condensates" with variable penetrance and mostly upon *SYP1* expression from an ectopic promoter (*GALs*), which could arise from its predicted propensity to form droplets. The biochemical nature of these "condensates" remains to be determined and is beyond the scope of this paper, but whether Syp1/FCHo2, alone or in combination with Ede1/Eps15, exploits liquid-liquid phase separation properties to modulate septin architecture is an exciting possibility for future studies. Furthermore, whether the activities of Syp1 in septin organization and endocytosis are linked or coordinated in yeast cells remains to be investigated.

Finally, given that yeast septins have a marked preference for micron-scale membrane curvatures,[86,87] Syp1 could also influence septin architecture *in vivo* through membrane bending at the bud neck. While the intrinsic curvature of F-BAR domains is able to induce nanometer-scale membrane curvatures (i.e., in a range that is unlikely to enhance septin recruitment), disordered domains have been shown to be potent drivers of membrane bending and generate shallower curvatures than those induced by BAR proteins.[88–90]

In summary, we have uncovered the molecular function of Syp1 in budding yeast septin organization and dynamics. Given its conservation, it will be of great interest to investigate if its mammalian counterparts FCHo1/2, as well as other structurally related proteins, control septin architecture *in vivo*.

Limitations of the study

First, although our data indicate that Syp1 could have a binding preference for Cdc11-capped octamers relative to Shs1-capped octamers, we do not know how this specificity is achieved at the molecular level, mainly because the interaction interface between Syp1 and septins is not known. Second, while we show here that Syp1 is able to bundle septin filaments *in vitro*, how exactly it contributes to septin collar organization at the bud neck of yeast cells remains to be established. Third, whether the ectopic clusters caused by forced Syp1-septin interaction at the mother cell plasma membrane are genuine septin filament bundles remains a hypothesis so far. Further structural analyses and ultrastructural microscopy techniques (e.g., correlative light and electron microscopy) will be required to address these questions.

STAR★METHODS

Detailed methods are provided in the online version of this paper and include the following:

- KEY RESOURCES TABLE
- RESOURCE AVAILABILITY
  - Lead contact
  - Materials availability
  - Data and code availability
- EXPERIMENTAL MODEL AND SUBJECT DETAILS
  - Strains, growth conditions, primers and plasmids
- METHOD DETAILS
  - Live cell imaging
  - Protein purification
  - Transmission electron microscopy
  - Cryo-electron microscopy
  - Dynamic light scattering (DLS)
  - Circular dichroism
  - Supported lipid bilayers and sub-diffraction fluorescence microscopy
  - Atomic force microscopy
- QUANTIFICATION AND STATISTICAL ANALYSIS

AUTHOR CONTRIBUTIONS

Conceptualization: S.P. and S.I. Investigation: S.I., F.E.A., L.C., and S.P. Methodology: S.I., F.E.A., J.L.-K.-H., C.C., F.H., S.L., P.B., L.C., L.P., and S.P.

Visualization: S.I., F.E.A., L.P., and S.P. Supervision: S.P. and L.P. Funding acquisition: S.P. and L.P. Writing: S.P. with inputs from S.I, L.P., L.C., and P.B.

REFERENCES

1. Hartwell, L.H. (1971). Genetic control of the cell division cycle in yeast. IV. Genes controlling bud emergence and cytokinesis. Exp. Cell Res. *69*, 265–276.

2. Auxier, B., Dee, J., Berbee, M.L., and Momany, M. (2019). Diversity of opisthokont septin proteins reveals structural constraints and conserved motifs. BMC Evol. Biol. *19*, 4. https://doi.org/10.1186/s12862-018-1297-8.

3. Barral, Y. (2010). Cell biology. Septins at the nexus. Science *329*, 1289–1290. https://doi.org/10.1126/science.1195445.

4. Mostowy, S., and Cossart, P. (2012). Septins: the fourth component of the cytoskeleton. Nat. Rev. Mol. Cell Biol. *13*, 183–194. https://doi.org/10.1038/nrm3284.

5. Bhavsar-Jog, Y.P., and Bi, E. (2017). Mechanics and regulation of cytokinesis in budding yeast. Semin. Cell Dev. Biol. *66*, 107–118. https://doi.org/10.1016/j.semcdb.2016.12.010.

6. Juanes, M.A., and Piatti, S. (2016). The final cut: cell polarity meets cytokinesis at the bud neck in S. cerevisiae. Cell. Mol. Life Sci. *73*, 3115–3136. https://doi.org/10.1007/s00018-016-2220-3.

7. Founounou, N., Loyer, N., and Le Borgne, R. (2013). Septins regulate the contractility of the actomyosin ring to enable adherens junction remodeling during cytokinesis of epithelial cells. Dev. Cell *24*, 242–255. https://doi.org/10.1016/j.devcel.2013.01.008.

8. Karasmanis, E.P., Hwang, D., Nakos, K., Bowen, J.R., Angelis, D., and Spiliotis, E.T. (2019). A septin double ring controls the spatiotemporal organization of the ESCRT machinery in cytokinetic abscission. Curr. Biol. *29*, 2174–2182.e7. https://doi.org/10.1016/j.cub.2019.05.050.

9. Bridges, A.A., and Gladfelter, A.S. (2015). Septin form and function at the cell cortex. J. Biol. Chem. *290*, 17173–17180. https://doi.org/10.1074/jbc.R114.634444.

10. Caudron, F., and Barral, Y. (2009). Septins and the lateral compartmentalization of eukaryotic membranes. Dev. Cell *16*, 493–506.

11. Spiliotis, E.T., and Nakos, K. (2021). Cellular functions of actin- and microtubule-associated septins. Curr. Biol. *31*, R651–R666. https://doi.org/10.1016/j.cub.2021.03.064.

12. Bertin, A., McMurray, M.A., Grob, P., Park, S.S., Garcia, G., 3rd, Patanwala, I., Ng, H.L., Alber, T., Thorner, J., and Nogales, E. (2008). Saccharomyces cerevisiae septins: supramolecular organization of heterooligomers and the mechanism of filament assembly. Proc. Natl. Acad. Sci. USA *105*, 8274–8279. https://doi.org/10.1073/pnas.0803330105.

13. Bertin, A., McMurray, M.A., Thai, L., Garcia, G., 3rd, Votin, V., Grob, P., Allyn, T., Thorner, J., and Nogales, E. (2010). Phosphatidylinositol-4,5-bisphosphate promotes budding yeast septin filament assembly and organization. J. Mol. Biol. *404*, 711–731. https://doi.org/10.1016/j.jmb.2010.10.002.

14. Bridges, A.A., Zhang, H., Mehta, S.B., Occhipinti, P., Tani, T., and Gladfelter, A.S. (2014). Septin assemblies form by diffusion-driven annealing on membranes. Proc. Natl. Acad. Sci. USA *111*, 2146–2151. https://doi.org/10.1073/pnas.1314138111.

15. Farkasovsky, M., Herter, P., Voß, B., and Wittinghofer, A. (2005). Nucleotide binding and filament assembly of recombinant yeast septin complexes. Biol. Chem. *386*, 643–656. https://doi.org/10.1515/BC.2005.075.

16. Field, C.M., al-Awar, O., Rosenblatt, J., Wong, M.L., Alberts, B., and Mitchison, T.J. (1996). A purified Drosophila septin complex forms filaments and exhibits GTPase activity. J. Cell Biol. *133*, 605–616. https://doi.org/10.1083/jcb.133.3.605.

17. Frazier, J.A., Wong, M.L., Longtine, M.S., Pringle, J.R., Mann, M., Mitchison, T.J., and Field, C. (1998). Polymerization of purified yeast septins: evidence that organized filament arrays may not be required for septin function. J. Cell Biol. *143*, 737–749.

18. Kinoshita, M., Field, C.M., Coughlin, M.L., Straight, A.F., and Mitchison, T.J. (2002). Self- and actin-templated assembly of mammalian septins. Dev. Cell *3*, 791–802. https://doi.org/10.1016/S1534-5807(02)00366-0.

19. Mendoza, M., Hyman, A.A., and Glotzer, M. (2002). GTP binding induces filament assembly of a recombinant septin. Curr. Biol. *12*, 1858–1863. https://doi.org/10.1016/s0960-9822(02)01258-7.

20. Szuba, A., Bano, F., Castro-Linares, G., Iv, F., Mavrakis, M., Richter, R.P., Bertin, A., and Koenderink, G.H. (2021). Membrane binding controls ordered self-assembly of animal septins. Elife *10*, e63349. https://doi.org/10.7554/eLife.63349.

21. Versele, M., Gullbrand, B., Shulewitz, M.J., Cid, V.J., Bahmanyar, S., Chen, R.E., Barth, P., Alber, T., and Thorner, J. (2004). Protein-protein interactions governing septin heteropentamer assembly and septin filament organization in Saccharomyces cerevisiae. Mol. Biol. Cell *15*, 4568–4583. https://doi.org/10.1091/mbc.e04-04-0330.

22. Zhang, J., Kong, C., Xie, H., McPherson, P.S., Grinstein, S., and Trimble, W.S. (1999). Phosphatidylinositol polyphosphate binding to the mammalian septin H5 is modulated by GTP. Curr. Biol. *9*, 1458–1467.

23. Valadares, N.F., d' Muniz Pereira, H., Ulian Araujo, A.P., and Garratt, R.C. (2017). Septin structure and filament assembly. Biophys Rev. *9*, 481–500. https://doi.org/10.1007/s12551-017-0320-4.

24. Weirich, C.S., Erzberger, J.P., and Barral, Y. (2008). The septin family of GTPases: architecture and dynamics. Nat. Rev. Mol. Cell Biol. *9*, 478–489.

25. Garcia, G., 3rd, Bertin, A., Li, Z., Song, Y., McMurray, M.A., Thorner, J., and Nogales, E. (2011). Subunit-dependent modulation of septin assembly: budding yeast septin Shs1 promotes ring and gauze formation. J. Cell Biol. *195*, 993–1004. https://doi.org/10.1083/jcb.201107123.

26. Mino, A., Tanaka, K., Kamei, T., Umikawa, M., Fujiwara, T., and Takai, Y. (1998). Shs1p: a novel member of septin that interacts with Spa2p, involved in polarized growth inSaccharomyces cerevisiae. Biochem. Biophys. Res. Commun. *251*, 732–736. https://doi.org/10.1006/bbrc.1998.9541.

27. McMurray, M.A., Bertin, A., Garcia, G., 3rd, Lam, L., Nogales, E., and Thorner, J. (2011). Septin filament formation is essential in budding yeast. Dev. Cell *20*, 540–549. https://doi.org/10.1016/j.devcel.2011.02.004.

28. Bertin, A., McMurray, M.A., Pierson, J., Thai, L., McDonald, K.L., Zehr, E.A., García, G., Peters, P., Thorner, J., and Nogales, E. (2012). Three-dimensional ultrastructure of the septin filament network in Saccharomyces cerevisiae. Mol. Biol. Cell *23*, 423–432. https://doi.org/10.1091/mbc.E11-10-0850.

29. Byers, B., and Goetsch, L. (1976). A highly ordered ring of membrane-associated filaments in budding yeast. J. Cell Biol. *69*, 717–721.

30. Demay, B.S., Bai, X., Howard, L., Occhipinti, P., Meseroll, R.A., Spiliotis, E.T., Oldenbourg, R., and Gladfelter, A.S. (2011). Septin filaments exhibit a dynamic, paired organization that is conserved from yeast to mammals. J. Cell Biol. *193*, 1065–1081. https://doi.org/10.1083/jcb.201012143.

31. Ong, K., Wloka, C., Okada, S., Svitkina, T., and Bi, E. (2014). Architecture and dynamic remodelling of the septin cytoskeleton during the cell cycle. Nat. Commun. *5*, 5698. https://doi.org/10.1038/ncomms6698.

32. Vrabioiu, A.M., and Mitchison, T.J. (2006). Structural insights into yeast septin organization from polarized fluorescence microscopy. Nature *443*, 466–469.

33. Vrabioiu, A.M., and Mitchison, T.J. (2007). Symmetry of septin hourglass and ring structures. J. Mol. Biol. *372*, 37–49. https://doi.org/10.1016/j.jmb.2007.05.100.

34. Marquardt, J., Chen, X., and Bi, E. (2019). Architecture, remodeling, and functions of the septin cytoskeleton. Cytoskeleton *76*, 7–14. https://doi.org/10.1002/cm.21475.

35. Caviston, J.P., Longtine, M., Pringle, J.R., and Bi, E. (2003). The role of Cdc42p GTPase-activating proteins in assembly of the septin ring in yeast. Mol. Biol. Cell *14*, 4051–4066.

36. Gladfelter, A.S., Bose, I., Zyla, T.R., Bardes, E.S., and Lew, D.J. (2002). Septin ring assembly involves cycles of GTP loading and hydrolysis by Cdc42p. J. Cell Biol. *156*, 315–326. https://doi.org/10.1083/jcb.200109062.

37. Iwase, M., Luo, J., Nagaraj, S., Longtine, M., Kim, H.B., Haarer, B.K., Caruso, C., Tong, Z., Pringle, J.R., and Bi, E. (2006). Role of a Cdc42p effector pathway in recruitment of the yeast septins to the presumptive bud site. Mol. Biol. Cell *17*, 1110–1125. https://doi.org/10.1091/mbc.E05-08-0793.

38. Okada, S., Leda, M., Hanna, J., Savage, N.S., Bi, E., and Goryachev, A.B. (2013). Daughter cell identity emerges from the interplay of cdc42, septins, and exocytosis. Dev. Cell *26*, 148–161. https://doi.org/10.1016/j.devcel.2013.06.015.

39. Dobbelaere, J., and Barral, Y. (2004). Spatial coordination of cytokinetic events by compartmentalization of the cell cortex. Science *305*, 393–396.

40. Lippincott, J., Shannon, K.B., Shou, W., Deshaies, R.J., and Li, R. (2001). The Tem1 small GTPase controls actomyosin and septin dynamics during cytokinesis. J. Cell Sci. *114*, 1379–1386.

41. Wloka, C., Nishihama, R., Onishi, M., Oh, Y., Hanna, J., Pringle, J.R., Krauss, M., and Bi, E. (2011). Evidence that a septin diffusion barrier is dispensable for cytokinesis in budding yeast. Biol. Chem. *392*, 813–829. https://doi.org/10.1515/BC.2011.083.

42. Tamborrini, D., Juanes, M.A., Ibanes, S., Rancati, G., and Piatti, S. (2018). Recruitment of the mitotic exit network to yeast centrosomes couples septin displacement to actomyosin constriction. Nat. Commun. *9*, 4308. https://doi.org/10.1038/s41467-018-06767-0.

43. Booth, E.A., Sterling, S.M., Dovala, D., Nogales, E., and Thorner, J. (2016). Effects of Bni5 binding on septin filament organization. J. Mol. Biol. *428*, 4962–4980. https://doi.org/10.1016/j.jmb.2016.10.024.

44. Marquardt, J., Yao, L.-L., Okada, H., Svitkina, T., and Bi, E. (2020). The LKB1-like kinase Elm1 controls septin hourglass assembly and stability by regulating filament pairing. Curr. Biol. *30*, 2386–2394.e4. https://doi.org/10.1016/j.cub.2020.04.035.

45. Patasi, C., Godocikova, J., Michlikova, S., Nie, Y., Kacerikova, R., Kvalova, K., Raunser, S., and Farkasovsky, M. (2015). The role of Bni5 in the regulation of septin higher-order structure formation. Biol. Chem. *396*, 1325–1337. https://doi.org/10.1515/hsz-2015-0165.

46. Sadian, Y., Gatsogiannis, C., Patasi, C., Hofnagel, O., Goody, R.S., Farkasovsky, M., and Raunser, S. (2013). The role of Cdc42 and Gic1 in the regulation of septin filament formation and dissociation. Elife *2*, e01085. https://doi.org/10.7554/eLife.01085.

47. Apel, A.R., Hoban, K., Chuartzman, S., Tonikian, R., Sidhu, S., Schuldiner, M., et al. (2017). Syp1 regulates the clathrin-mediated and clathrin-independent endocytosis of multiple cargo proteins through a novel sorting motif. Mol. Biol. Cell *28*, 2434–2448. https://doi.org/10.1091/mbc.e15-10-0731.

48. Boettner, D.R., D'Agostino, J.L., Torres, O.T., Daugherty-Clarke, K., Uygur, A., Reider, A., Wendland, B., Lemmon, S.K., and Goode, B.L. (2009). The F-BAR protein Syp1 negatively regulates WASp-Arp2/3 complex activity during endocytic patch formation. Curr. Biol. *19*, 1979–1987. https://doi.org/10.1016/j.cub.2009.10.062.

49. Reider, A., Barker, S.L., Mishra, S.K., Im, Y.J., Maldonado-Baez, L., Hurley, J.H., Traub, L.M., and Wendland, B. (2009). Syp1 is a conserved endocytic adaptor that contains domains involved in cargo selection and membrane tubulation. EMBO J. *28*, 3103–3116. https://doi.org/10.1038/emboj.2009.248.

50. Stimpson, H.E., Toret, C.P., Cheng, A.T., Pauly, B.S., and Drubin, D.G. (2009). Early-arriving Syp1p and Ede1p function in endocytic site placement and formation in budding yeast. Mol. Biol. Cell *20*, 4640–4651. https://doi.org/10.1091/mbc.E09-05-0429.

51. Merlini, L., Bolognesi, A., Juanes, M.A., Vandermoere, F., Courtellemont, T., Pascolutti, R., Seveno, M., Barral, Y., and Piatti, S. (2015). Rho1- and Pkc1-dependent phosphorylation of the F-BAR protein Syp1 contributes to septin ring assembly. Mol. Biol. Cell *26*, 3245–3262. https://doi.org/10.1091/mbc.E15-06-0366.

52. Qiu, W., Neo, S.P., Yu, X., and Cai, M. (2008). A novel septin-associated protein, Syp1p, is required for normal cell cycle-dependent septin cytoskeleton dynamics in yeast. Genetics *180*, 1445–1457. https://doi.org/10.1534/genetics.108.091900.

53. McMurray, M.A., and Thorner, J. (2008). Septin stability and recycling during dynamic structural transitions in cell division and development. Curr. Biol. *18*, 1203–1208. https://doi.org/10.1016/j.cub.2008.07.020.

54. Moran, K.D., Kang, H., Araujo, A.V., Zyla, T.R., Saito, K., Tsygankov, D., et al. (2019). Cell-cycle control of cell polarity in yeast. J. Cell Biol. *218*, 171–189. https://doi.org/10.1083/jcb.201806196.

55. Renz, C., Oeljeklaus, S., Grinhagens, S., Warscheid, B., Johnsson, N., and Gronemeyer, T. (2016). Identification of cell cycle dependent interaction partners of the septins by quantitative mass spectrometry. PLoS One *11*, e0148340. https://doi.org/10.1371/journal.pone.0148340.

56. Falke, S., and Betzel, C. (2019). Dynamic light scattering (DLS). Radiation in Bioanalysis *8*, 173–193. https://doi.org/10.1007/978-3-030-28247-9_6.

57. Cipelletti, L., Manley, S., Ball, R.C., and Weitz, D.A. (2000). Universal aging features in the restructuring of fractal colloidal gels. Phys. Rev. Lett. *84*, 2275–2278. https://doi.org/10.1103/PhysRevLett.84.2275.

58. Zhao, H., Michelot, A., Koskela, E.V., Tkach, V., Stamou, D., Drubin, D.G., and Lappalainen, P. (2013). Membrane-sculpting BAR domains generate stable lipid microdomains. Cell Rep. *4*, 1213–1223. https://doi.org/10.1016/j.celrep.2013.08.024.

59. Erdős, G., and Dosztányi, Z. (2020). Analyzing protein disorder with IUPred2A. Curr. Protoc. Bioinformatics *70*, e99. https://doi.org/10.1002/cpbi.99.

60. Loya, T.J., O'Rourke, T.W., Simke, W.C., Kelley, J.B., and Reines, D. (2018). Nab3's localization to a nuclear granule in response to nutrient deprivation is determined by its essential prion-like domain. PLoS One *13*, e0209195. https://doi.org/10.1371/journal.pone.0209195.

61. O'Rourke, T.W., Loya, T.J., Head, P.E., Horton, J.R., and Reines, D. (2015). Amyloid-like assembly of the low complexity domain of yeast Nab3. Prion *9*, 34–47. https://doi.org/10.1080/19336896.2014.997618.

62. Dobbelaere, J., Gentry, M.S., Hallberg, R.L., and Barral, Y. (2003). Phosphorylation-dependent regulation of septin dynamics during the cell cycle. Dev. Cell *4*, 345–357.

63. Tarassov, K., Messier, V., Landry, C.R., Radinovic, S., Serna Molina, M.M., Shames, I., Malitskaya, Y., Vogel, J., Bussey, H., and Michnick, S.W. (2008). An in vivo map of the yeast protein interactome. Science *320*, 1465–1470. https://doi.org/10.1126/science.1153878.

64. Cabantous, S., Nguyen, H.B., Pedelacq, J.D., Koraichi, F., Chaudhary, A., Ganguly, K., Lockard, M.A., Favre, G., Terwilliger, T.C., and Waldo, G.S. (2013). A new protein-protein interaction sensor based on tripartite split-GFP association. Sci. Rep. *3*, 2854. https://doi.org/10.1038/srep02854.

65. Finnigan, G.C., Duvalyan, A., Liao, E.N., Sargsyan, A., and Thorner, J. (2016). Detection of protein-protein interactions at the septin collar in

Saccharomyces cerevisiae using a tripartite split-GFP system. Mol. Biol. Cell *27*, 2708–2725. https://doi.org/10.1091/mbc.E16-05-0337.

66. Rothbauer, U., Zolghadr, K., Muyldermans, S., Schepers, A., Cardoso, M.C., and Leonhardt, H. (2008). A versatile nanotrap for biochemical and functional studies with fluorescent fusion proteins. Mol. Cell. Proteomics *7*, 282–289. https://doi.org/10.1074/mcp.M700342-MCP200.

67. Mumberg, D., Muller, R., and Funk, M. (1994). Regulatable promoters of Saccharomyces cerevisiae: comparison of transcriptional activity and their use for heterologous expression. Nucleic Acids Res. *22*, 5767–5768. https://doi.org/10.1093/nar/22.25.5767.

68. Barral, Y., Parra, M., Bidlingmaier, S., and Snyder, M. (1999). Nim1-related kinases coordinate cell cycle progression with the organization of the peripheral cytoskeleton in yeast. Genes Dev. *13*, 176–187. https://doi.org/10.1101/gad.13.2.176.

69. Lew, D.J. (2003). The morphogenesis checkpoint: how yeast cells watch their figures. Curr. Opin. Cell Biol. *15*, 648–653. https://doi.org/10.1016/j.ceb.2003.09.001.

70. Longtine, M.S., Theesfeld, C.L., McMillan, J.N., Weaver, E., Pringle, J.R., and Lew, D.J. (2000). Septin-dependent assembly of a cell cycle-regulatory module in Saccharomyces cerevisiae. Mol. Cell Biol. *20*, 4049–4061. https://doi.org/10.1128/MCB.20.11.4049-4061.2000.

71. Boeke, D., Trautmann, S., Meurer, M., Wachsmuth, M., Godlee, C., Knop, M., and Kaksonen, M. (2014). Quantification of cytosolic interactions identifies Ede1 oligomers as key organizers of endocytosis. Mol. Syst. Biol. *10*, 756. https://doi.org/10.15252/msb.20145422.

72. Kozak, M., and Kaksonen, M. (2022). Condensation of Ede1 promotes the initiation of endocytosis. Elife *11*, e72865. https://doi.org/10.7554/eLife.72865.

73. Wilfling, F., Lee, C.-W., Erdmann, P.S., Zheng, Y., Sherpa, D., Jentsch, S., Pfander, B., Schulman, B.A., and Baumeister, W. (2020). A selective autophagy pathway for phase-Separated endocytic protein deposits. Mol. Cell *80*, 764–778.e7. https://doi.org/10.1016/j.molcel.2020.10.030.

74. Henne, W.M., Kent, H.M., Ford, M.G.J., Hegde, B.G., Daumke, O., Butler, P.J.G., Mittal, R., Langen, R., Evans, P.R., and McMahon, H.T. (2007). Structure and analysis of FCHo2 F-BAR domain: a dimerizing and membrane recruitment module that effects membrane curvature. Structure *15*, 839–852. https://doi.org/10.1016/j.str.2007.05.002.

75. Pietrosemoli, N., Pancsa, R., and Tompa, P. (2013). Structural disorder provides increased adaptability for vesicle trafficking pathways. PLoS Comput. Biol. *9*, e1003144. https://doi.org/10.1371/journal.pcbi.1003144.

76. Wright, P.E., and Dyson, H.J. (2015). Intrinsically disordered proteins in cellular signalling and regulation. Nat. Rev. Mol. Cell Biol. *16*, 18–29. https://doi.org/10.1038/nrm3920.

77. Tompa, P. (2012). On the supertertiary structure of proteins. Nat. Chem. Biol. *8*, 597–600. https://doi.org/10.1038/nchembio.1009.

78. Hegyi, H., Schad, E., and Tompa, P. (2007). Structural disorder promotes assembly of protein complexes. BMC Struct. Biol. *7*. https://doi.org/10.1186/1472-6807-7-65.

79. Shoemaker, B.A., Portman, J.J., and Wolynes, P.G. (2000). Speeding molecular recognition by using the folding funnel: the fly-casting mechanism. Proc. Natl. Acad. Sci. USA *97*, 8868–8873. https://doi.org/10.1073/pnas.160259697.

80. Marcoux, N., Cloutier, S., Zakrzewska, E., Charest, P.-M., Bourbonnais, Y., and Pallotta, D. (2000). Suppression of the profilin-deficient phenotype by the RHO2 signaling pathway in *Saccharomyces cerevisiae*. Genetics *156*, 579–592. https://doi.org/10.1093/genetics/156.2.579.

81. Wright, P.E., and Dyson, H.J. (2009). Linking folding and binding. Curr. Opin. Struct. Biol. *19*, 31–38. https://doi.org/10.1016/j.sbi.2008.12.003.

82. Chen, H., Fre, S., Slepnev, V.I., Capua, M.R., Takei, K., Butler, M.H., Di Fiore, P.P., and De Camilli, P. (1998). Epsin is an EH-domain-binding protein implicated in clathrin-mediated endocytosis. Nature *394*, 793–797. https://doi.org/10.1038/29555.

83. Henne, W.M., Boucrot, E., Meinecke, M., Evergren, E., Vallis, Y., Mittal, R., and McMahon, H.T. (2010). FCHo proteins are nucleators of clathrin-mediated endocytosis. Science *328*, 1281–1284. https://doi.org/10.1126/science.1188462.

84. Ma, L., Umasankar, P.K., Wrobel, A.G., Lymar, A., McCoy, A.J., Holkar, S.S., Jha, A., Pradhan-Sundd, T., Watkins, S.C., Owen, D.J., et al. (2016). Transient fcho1/2•Eps15/R•AP-2 nanoclusters prime the AP-2 clathrin adaptor for cargo binding. Dev. Cell *37*, 428–443. https://doi.org/10.1016/j.devcel.2016.05.003.

85. Day, K.J., Kago, G., Wang, L., Richter, J.B., Hayden, C.C., Lafer, E.M., and Stachowiak, J.C. (2021). Liquid-like protein interactions catalyse assembly of endocytic vesicles. Nat. Cell Biol. *23*, 366–376. https://doi.org/10.1038/s41556-021-00646-5.

86. Beber, A., Taveneau, C., Nania, M., Tsai, F.-C., Di Cicco, A., Bassereau, P., Lévy, D., Cabral, J.T., Isambert, H., Mangenot, S., et al. (2019). Membrane reshaping by micrometric curvature sensitive septin filaments. Nat. Commun. *10*, 420. https://doi.org/10.1038/s41467-019-08344-5.

87. Bridges, A.A., Jentzsch, M.S., Oakes, P.W., Occhipinti, P., and Gladfelter, A.S. (2016). Micron-scale plasma membrane curvature is recognized by the septin cytoskeleton. J. Cell Biol. *213*, 23–32. https://doi.org/10.1083/jcb.201512029.

88. Busch, D.J., Houser, J.R., Hayden, C.C., Sherman, M.B., Lafer, E.M., and Stachowiak, J.C. (2015). Intrinsically disordered proteins drive membrane curvature. Nat. Commun. *6*, 7875. https://doi.org/10.1038/ncomms8875.

89. Frost, A., Unger, V.M., and De Camilli, P. (2009). The BAR domain Superfamily: membrane-molding macromolecules. Cell *137*, 191–196. https://doi.org/10.1016/j.cell.2009.04.010.

90. Snead, W.T., Zeno, W.F., Kago, G., Perkins, R.W., Richter, J.B., Zhao, C., et al. (2019). BAR scaffolds drive membrane fission by crowding disordered domains. J. Cell Biol. *218*, 664–682. https://doi.org/10.1083/jcb.201807119.

91. Tudek, A., Porrua, O., Kabzinski, T., Lidschreiber, M., Kubicek, K., Fortova, A., Lacroute, F., Vanacova, S., Cramer, P., Stefl, R., et al. (2014). Molecular basis for coordinating transcription termination with noncoding RNA degradation. Mol. Cell *55*, 467–481. https://doi.org/10.1016/j.molcel.2014.05.031.

92. Káčeriková, R., Godočíková, J., Wang, Z., Kutejová, E., Raunser, S., and Farkašovský, M. (2018). Modulation of septin higher-order structure by the Cdc28 protein kinase. Biologia *73*, 1025–1033. https://doi.org/10.2478/s11756-018-0116-4.

93. El Alaoui, F., Casuso, I., Sanchez-Fuentes, D., Arpin-Andre, C., Rathar, R., Baecker, V., Castro, A., Lorca, T., Viaud, J., Vassilopoulos, S., et al. (2022). Structural organization and dynamics of FCHo2 docking on membranes. Elife *11*, e73156. https://doi.org/10.7554/eLife.73156.

94. Voth, W.P., Olsen, A.E., Sbia, M., Freedman, K.H., and Stillman, D.J. (2005). ACE2, CBK1, and BUD4 in budding and cell separation. Eukaryot. Cell *4*, 1018–1028. https://doi.org/10.1128/EC.4.6.1018-1028.2005.

95. Sheff, M.A., and Thorn, K.S. (2004). Optimized cassettes for fluorescent protein tagging in Saccharomyces cerevisiae. Yeast *21*, 661–670. https://doi.org/10.1002/yea.1130.

96. El Masri, D., Pierno, M., Berthier, L., and Cipelletti, L. (2005). Ageing and ultra-slow equilibration in concentrated colloidal hard spheres. Journal of Physics: Condensed *17*, S3543. https://doi.org/10.1088/0953-8984/17/45/046.

97. Miles, A.J., Ramalli, S.G., and Wallace, B.A. (2022). DichroWeb, a website for calculating protein secondary structure from circular dichroism spectroscopic data. Protein Sci. *31*, 37–46. https://doi.org/10.1002/pro.4153.

98. Picas, L., Rico, F., and Scheuring, S. (2012). Direct measurement of the mechanical properties of lipid phases in supported bilayers. Biophys. J. *102*, L01–L03. https://doi.org/10.1016/j.bpj.2011.11.4001.

99. Schillers, H., Rianna, C., Schäpe, J., Luque, T., Doschke, H., Wälte, M., Uriarte, J.J., Campillo, N., Michanetzis, G.P.A., Bobrowska, J., et al. (2017). Standardized nanomechanical atomic force microscopy procedure (SNAP) for measuring Soft and biological samples. Sci. Rep. *7*, 5117. https://doi.org/10.1038/s41598-017-05383-0.

100. Nečas, D., and Klapetek, P. (2012). Gwyddion: an open-source software for SPM data analysis. Open Phys. *10*, 181–188. https://doi.org/10.2478/s11534-011-0096-2.

101. Schneider, C.A., Rasband, W.S., and Eliceiri, K.W. (2012). NIH Image to ImageJ: 25 years of image analysis. Nat. Methods *9*, 671–675. https://doi.org/10.1038/nmeth.2089.

102. Bogovic, J.A., Hanslovsky, P., Wong, A., and Saalfeld, S. (2016). Robust registration of calcium images by learned contrast synthesis. In 2016 IEEE 13th International Symposium on Biomedical Imaging (ISBI), pp. 1123–1126. https://doi.org/10.1109/ISBI.2016.7493463.

STAR★METHODS

KEY RESOURCES TABLE

REAGENT or RESOURCE	SOURCE	IDENTIFIER
Chemicals, peptides, and recombinant proteins		
Agar	Formedium	Cat#AGA03
D(+)-Galactose	Formedium	Cat#GAL03
D(+)-Glucose anydrous	Formedium	Cat#GLU03
Peptone	Formedium	Cat#PEP03
D(+)-Raffinose pentahydrate	Formedium	Cat#RAF04
Yeast extract	Formedium	Cat#YEA03
Autoinduction medium	Formedium	Cat#AIMTB0210
Ampicillin	Euromedex	Cat#EU0400
Kanamycin Disulfate	Sigma-Aldrich	Cat#K1876
Chloramphenicol	MP Biomedicals	Cat#190321
FM4-64	ThermoFisher Scientific	Cat#T13320
Isopropyl β-D-thiogalactoside	Sigma-Aldrich	Cat#I6758
Lysozyme	Sigma-Aldrich	Cat#62970
Protease inhibitor Cocktail tablets	Roche	Cat#05892791001
Amylose resine	New England Biolabs	Cat#E8022
Thrombin	Serva	Cat#36402
Ni-NTA agarose beads	Qiagen	Cat#30210
Imidazol	Sigma-Aldrich	Cat#I5513
D-(+)-Maltose monohydrate	Sigma-Aldrich	Cat#5885
Lipid free-BSA	Sigma-Aldrich	Cat#A8806
Uranyl Acetate	SPI-Chem	Cat#2625
DOPE-Rhodamine	Avanti Polar Lipids	Cat#810150P
DOPC	Avanti Polar Lipids	Cat#850375P
DGS-NTA(Ni)	Avanti Polar Lipids	Cat#790404P
Septins, Syp1, FCHo2, Nab3 proteins (See STAR Methods)		
Deposited data		
Saccharomyces genome database		https://www.yeastgenome.org/
Experimental models: Organisms/strains		
S. cerevisiae: Strain background: W303 (*ade2-1, trp1-1, leu2-3,112, his3-11, 15, ura3*)	ATCC	ATTC: 208,353
BL21(DE3) chemically competent cells (*E. coli B dcm ompT hsdS*(r$_B^-$m$_B^-$) *gal*)	New England Biolabs	Cat#C2527H
Oligonucleotides		
Primers for PCR, see Table S2		
Recombinant DNA		
NAB3-His6 cloned in pET41a-derived plasmid	Domenico Libri Lab[91]	pDL469
colE1, AmpR, His6-CDC11, CDC10	M. Farkasovsky Lab[15,92]	pFM453
MBP-CDC12, His6-CDC3 cloned in p15A	M. Farkasovsky Lab[15,92]	pFM455
MBP-CDC12, His6-CDC3-yeGFP cloned in p15A	M. Farkasovsky Lab[15,92]	pFM873
C/U::SYP1(1-870) cloned in pET28a	B. Wendland Lab[49]	pBW1447

(Continued on next page)

Continued

REAGENT or RESOURCE	SOURCE	IDENTIFIER
C/U::syp1(1-264) cloned in pET28a	B. Wendland Lab[49]	pBW1451
C/U::syp1(265-565) cloned in pET28a	B. Wendland Lab[49]	pBW1504
C/U::syp1(566-870) cloned in pET28a	B. Wendland Lab[49]	pBW1041
syp1(1-565) cloned in pET28a	S. Piatti Lab stock	pSP1804
syp1(265-870) cloned in pET28a	S. Piatti Lab stock	pSP1805
Mouse full-length *FCHo2* (aa1-809) cloned in pET28a	Laura Picas Lab[93]	FCHo2
Software and algorithms		
ImageJ		https://imagej.nih.gov/ij/
Metamorph		http://www.meta.moleculardevices.com/
Dichroweb		http://dichroweb.cryst.bbk.ac.uk
Gwyddion		http://gwyddion.net/
Other		
HiTrap Chelating HP column	GE Healthcare	Cat#17-0409-01
HiLoad 16/60 Superdex 200 pg column	GE Healthcare	Cat#19-1069-01
Poly-Prep Chromatography Columns	Bio-Rad	Cat#7311550
Vivaspin 6 Centrifugal Concentrator 10000 MWCO	Sartorius	Cat#VS0601
Vivaspin 6 Centrifugal Concentrator 50000 MWCO	Sartorius	Cat#VS0631
Slide-A-Lyzer Dialysis Cassette 10000 MWCO	Thermo Scientific	Cat#87731
CelluSep Regenerated Cellulose Tubular Membranes 10000 MWCO	Chen Shuo Biotechnology	Cat#1005-32
Culture-Inserts 2 Well	Ibidi	Cat#80209
Fomvar carbon-coated grids	Delta Microscopies	Cat#FCF100-Cu
Lacey Carbon Type-A, 300 mesh, Copper grids	Ted Pella	Cat#01890
FluoroDishes	World Precision Instruments	Cat#FD35

RESOURCE AVAILABILITY

Lead contact
Further information and requests for resources and reagents should be directed to and will be fulfilled by the lead contact, Simonetta Piatti (simonetta.piatti@crbm.cnrs.fr).

Materials availability
All yeast strains and plasmids used in this study will be made available upon request without any restriction.

Data and code availability
- All data reported in this paper will be shared by the lead contact upon request.
- The study did not generate any unique code.
- Any additional information required to reanalyze the data reported in this paper is available from the lead contact upon request.

EXPERIMENTAL MODEL AND SUBJECT DETAILS

Strains, growth conditions, primers and plasmids
All yeast strains (Table S1) are congenic to W303 (*ade2-1, trp1-1, leu2-3,112, his3-11, 15 ura3*). W303 bears a single nucleotide deletion in the *BUD4* gene (*bud4-G2459fs*) that results in a premature stop codon. The *bud4-G2459fs* gene produces a truncated protein of 838 amino acids that lacks 609 amino acids and carries 18 non-natural amino acids at C-terminus (https://www.yeastgenome.org).

This mutation leads to septin ring disassembly, instead of splitting, at mitotic exit.[41] In order to properly visualize septin ring splitting, the genotype of yeast strains has been corrected to carry full length *BUD4* whenever pertinent.[42,94]

Yeast cultures were grown at 30°C in either synthetic medium (SD) supplemented with the appropriate nutrients or YEP (1% yeast extract, 2% bactopeptone, 50 mg/L adenine) medium. Raffinose was supplemented to 2%, glucose to 2% and galactose to 1%.

One-step tagging techniques were used to generate strains bearing *SYP1* or *SHS1* deletion, eGFP-tagged *SYP1*, either full length or truncated variants, GBD-tagged *CDC10*, as well as to tag septins with Dendra2.[95] A flexible linker of 6 glycines was introduced between the last amino acid of septins and Dendra2. The complete list of primers used in this study can be found in Table S2.

Plasmids for bacterial expression of Syp1, as well as its F-BAR, middle and μHD domains were previously described.[49] The plasmid for bacterial expression of *SYP1* F-BAR domain and middle region (aa 1-565; pSP1804) was constructed by amplifying a DNA fragment comprising the first 1778 bp of *SYP1* ORF with primers MP1473 and MP1474, followed by its cloning into NcoI/BamHI of pET28a. The plasmid for bacterial expression of *SYP1* middle region and μHD domain (aa 265-870; pSP1805) was constructed by amplifying a DNA fragment from 793bp to 2613bp of *SYP1* ORF with primers MP1475 and MP1476, followed by its cloning into a NdeI/BamHI of a pET28a.

The plasmid for bacterial expression of mouse FCHo2 and budding yeast Nab3 have been previously described.[93,91]

METHOD DETAILS

Live cell imaging

Cells were mounted on 1% agarose pads in SD medium on Fluorodishes and filmed at controlled temperature (30°C) with a 100X 1.49 NA oil immersion objective mounted on a Nikon Eclipse Ti microscope equipped with an EMCCD Evolve 512 Camera (Photometrics) and iLAS[2] module (Roper Scientific) and controlled by Metamorph. Z stacks of 8-13 planes were acquired every 4 min with a step size of 0.4 μm and a binning of 1. Z stacks were max-projected with ImageJ or Metamorph. For photoconversion experiments, selected cells were illuminated with a 405 nm laser in a rectangular region surrounding the septin collar (100 iterations, thickness 1). Cells were then illuminated with a 561 nm laser and filmed at 30°C with a Nikon Eclipse Ti microscope equipped with an EMCCD Evolve 512 Camera (Photometrics) and iLAS[2] module (Roper Scientific) and controlled by Metamorph. Z stacks of 12 planes were acquired every 2 min for 3 h with a step size of 0.4 μm and a binning of 1.

Endomembrane staining was carried out by pulse-chasing the lipophilic dye FM4-64 (Invitrogen, Carlsbad, CA) as follows. *CDC10-GBD GALs-SYP1-eGFP* cells were grown in YEPR at 30°C to exponential phase and then induced with 1% galactose for 3 h. Cells were then placed on ice for 10 min to block endocytosis, and FM4-64 was added to cultures at the final concentration of 16 μM, followed by a 15 min incubation on ice. Cells were then washed with fresh SD containing raffinose and galactose before being mounted on 1% agarose pads in SD raffinose/galactose on Fluorodishes and imaged with a 63X 1.4 NA oil immersion objective mounted on a confocal Zeiss LSM980 Airyscan. Z stacks of 34 planes were acquired with a step size of 0.15 μm and max-projected with ImageJ.

Protein purification

For purification of Cdc11-capped septin octamers, *E.coli* strain BL21 (DE3) Rosetta cells were transformed with plasmid pFM453 (colE1, Amp[r], *CDC10, CDC11*) and pFM455 (p15A, Kan[r], *MBP-CDC12, His6-CDC3*) or with pFM453 and pFM873 (p15A, Kan[r], *MBP-CDC12, His6-CDC3-yeGFP*).[15,92] Cells were grown in LB containing 50 μg/mL of ampicillin, 25 μg/mL of kanamycin, 34 μg/mL of chloramphenicol, 0.2% glucose and induced at OD_{600} = 1 by addition of 0.2 mM IPTG. After 20h at 16°C, cells were harvested by centrifugation and resuspended in Buffer A (25 mM $NaHPO_4$ pH 7.8, 300 mM NaCl, 0.5 mM $MgCl_2$, 5% glycerol) supplemented with 5 mM β-mercaptoethanol, 1 mg/mL of lysozyme and a cocktail of protease inhibitors (Complete EDTA-free Roche). Cells were sonicated 3x with 1′30″ cycles of 8″ pulses/8″ ice and extracts cleared at 30,000 *g* for 30′ at 4°C. Lysates were incubated 2 h at 4°C with 1 mL of amylose resin (New England Biolabs), pre-washed 3x with buffer A, on a rotating wheel. After incubation with the protein extracts, the slurry was washed 3 times with buffer A and loaded on a Polyprep column (Bio-Rad). Fractions of 0.5 mL were eluted with buffer A supplemented with 10 mM maltose and quantified by Nanodrop. The most concentrated fractions were pulled together and MBP was cleaved from the complex using thrombin at 5 U/mg of protein overnight at 6°C. Proteins were then diluted in 10 mL of buffer B (25 mM $NaHPO_4$ pH 7.8, 300 mM NaCl, 0.5 mM $MgCl_2$, 5% glycerol, 0.1% Triton X-100, 6 mM imidazole) supplemented with 5 mM β-mercaptoethanol and incubated 2 h at 4°C with 1 mL of Ni-NTA agarose beads (Qiagen), pre-washed 3x with buffer B, on a rotating wheel. The slurry was then washed 3 times with buffer C (25 mM $NaHPO_4$ pH 7.8, 500 mM NaCl, 0.5 mM $MgCl_2$, 5% glycerol, 0.15% Triton X-100, 5 mM β-mercaptoethanol, 8 mM imidazole) and loaded on a Polyprep column (Bio-Rad). Fractions of 0.5 mL were eluted with buffer A supplemented with 200 mM imidazole and quantified by Nanodrop. The most concentrated fractions were dialyzed in a buffer containing 20 mM Tris-HCl pH 8.2, 300 mM NaCl, 0.2 mM $MgCl_2$ and 2 mM DTT. Proteins were finally concentrated through Amicon Ultra filter units (10 kDa cut-off).

For Syp1 purification, BL21 DE3 cells transformed with pBW1447 (pET28a C/U:*SYP1*(1-870)), pBW1451 (pET28a C/U:*syp1*(1-264)), pBW1504 (pET28a C/U:*syp1*(265-565)) or pBW1041 (pET28a C/U:*syp1*(566-870))[49] were grown in LB containing 25 μg/mL of kanamycin, 34 μg/mL of chloramphenicol and 0.2% glucose and induced with 0.2 mM IPTG 20h at 20°C. Cells were lysed in 20 mM HEPES pH 7.4, 300 mM NaCl, 0.1% Tween 20 containing 0.5 mg/mL of lysozyme and a cocktail of protease inhibitors (Complete EDTA-free Roche). Cells were sonicated 3x with 1′30″ cycles of 8″ pulses/8″ ice and extracts cleared at 30,000 *g* for 30′ at

4°C. Lysates were incubated 2 h with 1 mL of Ni-NTA agarose beads (Qiagen), pre-washed 3x with 20 mM HEPES pH 7.4, 300 mM NaCl, 10 mM imidazole at 4°C on a rotating wheel. After incubation with the protein extracts, the slurry was washed 3 times with 20 mM HEPES pH 7.4, 300 mM NaCl, 40 mM imidazole and loaded on a Polyprep column (Bio-Rad). Fractions of 0.5 mL were eluted with 20 mM HEPES pH 7.4, 300 mM NaCl, 250 mM imidazole and quantified by Nanodrop. The most concentrated fractions were dialyzed in a buffer containing 50 mM Tris-HCl pH 8, 50 mM NaCl. The protein was concentrated through Amicon Ultra filter units (50 kDa cut-off for full-length Syp1 or 10kDa cut-off for the truncated forms of Syp1).

Mouse FCHo2 was purified as recently described.[93] Briefly, BL21 DE3 cells transformed with pET28a(3C)[93] were grown to OD = 0.6–0.8 in 1L of LB containing 25 μg/mL of kanamycin and 34 μg/mL of chloramphenicol and induced with 0.5 mM IPTG at 25°C overnight. Bacteria were lysed in ice in cold lysis buffer (20 mM HEPES pH 7.5, 150 mM NaCl, 0.5% Triton X-100 containing 0.5 mg/mL of lysozyme and a cocktail of protease inhibitors (Complete EDTA-free Roche)). Cells were sonicated for 10 min with 30″ pulses/30″ ice and extracts cleared at 20,000 g for 30′ at 4°C. Lysates were filtered (0.45 μm pores) and applied at 1 mL/min (AKTA chromatography) to 5 mL of HiTrap Chelating HP column (GE Healthcare), pre-washed with 5 volumes of H_2O and 5 volumes of binding buffer (20 mM HEPES pH 7.5, 150 mM NaCl). The slurry was washed at 1 mL/min with 20 mM Hepes pH 7.5, 150 mM NaCl, 50 mM imidazole and eluted with 20 mM Hepes pH 7.5, 150 mM NaCl, 250 mM imidazole. The protein was concentrated through Amicon Ultra filter units (10 kDa cut-off), quantified by Bradford and dialysed in 20 mM Hepes pH 7.5, 150 mM NaCl for immediate usage.

Nab3 was purified according to.[91] BL21 DE3 cells transformed with pDL469-Nab3-His6[91] were grown to OD = 0.8-1 in 500 mL of autoinduction medium (Formedium) containing 25 μg/mL of kanamycin and 34 μg/mL of chloramphenicol at 20°C overnight. Bacteria were lysed in ice in 25 mL of cold lysis buffer (50 mM Tris-Cl pH 7.5, 500 mM NaCl, 5% glycerol, 1 mM DTT, 20 mM imidazole and containing 0.05 mg/mL of lysozyme and a cocktail of protease inhibitors (Complete EDTA-free Roche)). Cells were sonicated with 15-20 cycles of 15″ pulses/45″ ice and extracts cleared at 20,000 g for 30′ at 4°C. The cleared lysate was filtered (0.45 μm pores) and applied at a flow rate of 1 mL/min (AKTA chromatography) to a HiTrap Chelating HP column (GE Healthcare), pre-washed with 10 volumes of distilled water and equilibrated with 10 volumes of buffer B (50 mM Tris-Cl pH 7.5, 500 mM NaCl, 5% glycerol) containing 20 mM imidazole (flow rate 2 mL/min). The resin was washed with 10 volumes of buffer B containing 20 mM imidazole (1 mL/min) and 10 volumes of buffer B containing 50 mM imidazole (1 mL/min) followed by elution with 20 volumes of a gradient of 50-300 mM imidazole in buffer B (1 mL/min). Fractions containing Nab3-His6, as estimated by SDS page electrophoresis, were pooled together and loaded on a HiLoad 16/60 Superdex 200 prep grade gel filtration column (1 mL/min, AKTA chromatography) prewashed with 2 volumes of distilled water and 2 volumes of gel filtration buffer (50 mM Tris-HCl pH 7.5, 500 mM NaCl, 50 mM imidazole, 5% glycerol) containing 50 mM imidazole. Nab3-His6 was eluted with 1–1.5 volumes of gel filtration buffer containing 50 mM imidazole. Fractions containing Nab3-His6 were pooled together and dialyzed overnight with CelluSep dialysis membrane against 2 L of storage buffer (50 mM Tris-Cl pH 7.5, 300 mM NaCl, 1mM DTT). The protein was then concentrated through Amicon Ultra filter units (10 kDa cut-off), quantified, flash-frozen in liquid N_2 and stored at −80°C.

Transmission electron microscopy

In general, septin polymerization in solution was induced by lowering the salt concentration (from 300 mM to 30 mM NaCl). For Figures 2A, 2B, 5E and S2A Cdc11-capped septin octamers were diluted to 130 nM (final concentration) in either high salt (20 mM Tris-HCl pH 8.2, 300 mM NaCl, 2 mM MgCl2, 40 μM GDP) or low salt buffer (20 mM Tris-HCl pH 8.2, 30 mM NaCl, 2 mM MgCl2, 40 μM GDP) in the absence or presence of recombinant Syp1 (ratio 1:1, 1:0.5 or 1:0.25) and let polymerise for 30 min at 4°C. 4μL of sample were absorbed on a Formvar carbon-coated grid (Delta Microscopies FCF100-Cu) for 30 s. The grids were then negatively stained for 1 min using 2% uranyl acetate in water. Data were collected using a Tecnai F20 transmission electron microscope at 120KV and equipped with a Veleta camera.

For Figures 5F and S4C, Cdc11-capped septin octamers were diluted to 175 nM (final concentration) in low salt buffer (20 mM Tris-HCl pH 8.2, 30 mM NaCl, 2 mM MgCl2, 40 μM GTP) in the presence of truncated forms of Syp1 (ratio 1:0.25) or full-length Nab3 (ratio 1:0.25, 1:0.5, 1:1). 3 μL of samples were absorbed on glow-discharged formvar carbon-coated grids (Delta Microscopies FCF100-Cu) and stained with 1% uranyl acetate. Grids were observed using a JEOL 1400 Flash transmission electron microscope at 120kV. Micrographs were recorded using a One View camera (Gatan Inc.) at different magnifications.

Cryo-electron microscopy

Purified septin octamers were diluted to 0.125 mg/mL and mixed with purified Syp1 protein at 1:0.25 ratio in low salt buffer (20 mM Tris-HCl pH8.2, 30 mM NaCl, 2 mM MgCl2, 40 μM GDP). 4μL of samples were applied on glow-discharged Lacey 300 mesh copper grids (Ted Pella Inc.), blotted for 3-4 s, and then flash-frozen in liquid ethane using the semi-automated plunge freezing device Vitrobot Mark IV (ThermoFisher Scientific) maintained at 100% relative humidity and 22°C. Images of frozen-hydrated samples were recorded on a JEOL 2200FS FEG TEM, operating at 200 kV under low-dose conditions (total dose of 20 electrons/$\mathring{A}^2$) in the zero–energy loss mode with a slit width of 20 eV. Images were recorded on a 4 K × 4 K slow-scan charge-coupled device camera (Gatan Inc.) at a nominal magnification of ×50,000 with defocus values ranging from 1.0 to 2.5 μm.

Dynamic light scattering (DLS)

For dynamic light scattering, we used a commercial DLS set-up (Figure 2F, Amtec Goniometer and Brookhaven BI-9000AT correlator) and a custom multi-speckle apparatus (Figure 2G),[96] both set at a detection angle of 90° and operated with a laser

with λ = 532 nm. Recombinant septin octamers at 160 nM were polymerised in solution by lowering the salt concentration to 30 mM NaCl in the absence or presence of 50% mol of recombinant Syp1. As it is usually done in DLS for analysing polydisperse samples, in Figure 2F we assumed that the field correlation function g_1 is the superposition of exponentially relaxing modes. Intensity and field correlation functions are related by $g_2(t)$-1 = $g_1(t)^2$ (Siegert relation). Accordingly, we used the following fitting function:

$$g_2(\tau) - 1 = B + \left[\sum_{n=1}^{13} A_n e^{-\frac{t}{\tau_n}} \right]^2$$, with τ_n the relaxation time of the n-th mode, A_n its amplitude and $B \leq 6 \ 10^{-4}$ a base line term due to experimental noise.

Circular dichroism

CD spectra were obtained using a ChiralScan spectrometer (Applied Photophysics, Leatherhead, Surrey, UK) under N_2. The mix of septin octamers with each individual Syp1 domain was diluted in 50 mM Tris-HCl pH8, 50 mM NaCl to the following final concentrations: 0.4 mg/mL for the F-BAR domain; 0.0125 mg/mL for the middle region; 0.5 mg/mL for the μHD. Samples (50 μL) were loaded into optically matched quartz cuvettes (0.2 cm path length; model 106-QS P, Hellma Analytics, USA) and CD spectra were measured at 20°C. Far-UV CD spectra were recorded 10 times from 190 to 250 nm at 1 nm increments. The background spectrum of buffer without protein was subtracted from the averaged protein spectra. Analysis of the spectra to extrapolate secondary structures was performed by Dichroweb (http://dichroweb.cryst.bbk.ac.uk).[97]

Supported lipid bilayers and sub-diffraction fluorescence microscopy

Glass coverslips were cleaned by sequential 30 min sonication steps, 1) in 1 M NaOH, 2) in 100% ethanol and 3) in milliQ water, with water rinsing between each step. Coverslips were finally plasma cleaned just before using. Supported lipid bilayers were composed of 95,8% (w/w) DOPC, 4% (w/w) DGS-NTA(Ni), 0.2% (w/w) Rhodamine-PE. Lipids dissolved in methanol/chloroform were mixed and dried for 1h in a vacuum oven at 60°C. Small unilamellar vesicles (SUVs, diameter ∼100nm) were obtained by extrusion of multila-mellar vesicles in citrate buffer (citrate 20 mM pH 4,6, KCl 50 mM, EGTA 0.5 mM) heated to 44°C.

40 μL of SUVs were deposit on a two-well silicone insert (IBIDI) and incubated 1 h at 40°C. Bilayers were carefully rinsed with wash buffer (20 mM Tris-HCl pH8, 300 mM NaCl) and then equilibrated with equilibration buffer (20 mM Tris-HCl pH 8, 50 mM NaCl, 1 mg/mL lipid-free BSA). Cdc11-capped yeGFP-tagged septin octamers were diluted to 100 nM in low salt buffer (20 mM Tris-HCl pH 8.2, 30 mM NaCl, 2 mM MgCl2, 40 μM GTP) and mixed with purified FCHo2, Syp1-BFP protein or its BFP-tagged domains at various ratios for 30 min at room temperature. 20 μL of sample were applied on the lipid bilayer and immediately visualised with a Zeiss LSM880 Airyscan confocal microscope. Excitation sources used were: 405 nm diode laser, an Argon laser for 488 nm and 514 nm and a Helium/Neon laser for 633 nm. Acquisitions were performed on a 63x/1.4 objective. Multidimensional acquisitions were acquired via an Airyscan detector (32-channel GaAsP photomultiplier tube (PMT) array detector).

Atomic force microscopy

AFM experiments were performed on a JPK NanoWizard IV microscope (JPK Instruments-Bruker, Germany) mounted on an inverted NIKON Ti2-U microscope (Nikon Instruments, Japan). Images were acquired in Quantitative Imaging (QI) mode under a setpoint force of 250 pN, based on previous work.[98] Rectangular-shaped BL-AC40TS-C2 cantilevers (Olympus, Japan) with a nominal spring constant of 0.09 N·m^{-1} and a nominal tip radius of 8 nm was used under liquid conditions. Before each experiment, the cantilever spring constant and sensitivity were determined by the thermal noise method.[99] QI mapping was performed at 256 × 256 pixels/line at a scan rate of 9.4 kHz.

For AFM experiments, SLBs were prepared on 1M NaOH treated coverslips following the same experimental procedure detailed in the previous section. After 30 min incubation of 50 nM of septin-yeGFP filaments with or without 25 nM of Syp1, samples were mounted on the AFM imaging holder and imaged in 20 mM Tris pH8, 150 mM NaCl. Epi-fluorescence images of septin filaments were visualized using a NIKON CFI APO VC 100x/1.4 objective and a JENOPTIK Fluorescence ProgRes MFcool camera. Real-time overlay of AFM topography and fluorescence microscopy images of septin filaments was performed using the JPK DirectOverlay mode (JPK Instruments-Bruker, Germany).

AFM image processing and analysis was performed using the open-source software Gwyddion.[100] Correlative fluorescence and AFM image representation was performed using ImageJ[101] and the BigWarp plugin.[102]

QUANTIFICATION AND STATISTICAL ANALYSIS

The number of samples analyzed (n) is indicated in the figures or figure legends. Error bars correspond to standard deviations, as indicated in the figure legends. Mann–Whitney U test was used for statistical analysis and to assess the statistical significance of the observed differences.